Investigation of nanopore-spanning bilayer on silicon nitride and silicon oxide by utilizing phospholipid liposomes from *Escherichia coli* membrane lipids and soybean lecithin

Master thesis

Tri Huu Huynh

January 15, 2020

AALBORG UNIVERSITY
STUDENT REPORT

Final year of master studies of Nanobiotechnology at School of Engineering and Science

The Faculty of Natural Sciences

Physics and Nanotechnology
Skjernvej 4a
9220 Aalborg Ø

Title:

Investigation of nanopore-spanning bilayer on silicon nitride and silicon oxide by utilizing phospholipid liposomes from *Escherichia coli* membrane lipids and soybean lecithin.

Project period:

September 2018 - Dec 2019

Project group:

5.321

Participants:

Tri Huu Huynh

Supervisors:

Leonid Gurevich

Total pages: 59
Appendices: 0
Finalized 19-12-2019

Abstract:

In this project, formation of nanopore-spanning lipid bilayer on silicon and silicon oxide, by utilizing phospholipids from *Escherica coli* and soybean lecithin. Liposomes were produced and characterized. The liposomes were produced from extracted *E.coli* lipid membranes, while lecithin was already harvested. The liposomes were deposited on SiN_x and SiO_x nanopores. The presence of lipids was verified by using thin-layer chromatography (TLC) and the size of the liposomes was measured with dynamic light scattering (DLS) and gave a size of 164nm, 128nm, 122.6nm, and 32.67nm. The liposomes were also characterized with atomic force microscopy (AFM) to see the coverage as well as the morphology. Surface functionalization was done with APTMS to facilitate a hydrophilic surface. By using a dedicated kit the formation of nanopore-spanning lipid bilayers could be measured. Electrochemical measurements showed open square-waves for all the measurements indicating no formation were presence, It was suspected that leakage was present, but damaged o-rings were replaced.

Contents

1 Introduction

Biological membranes are complex structures consisting of many different lipids and protein that performs vital processes for the cell. To study these membranes, a reduction of parameters must be made. This drive to artificially mimic the cell has paved the way to many potential applications such as micromachine engineered to sense the environmental change. [1]. Due to phospholipids amphipathic, nature synthesised micelle and vesicle can be produced and these systems have been the leading candidate for drug delivery [2]. Phospholipid vesicles can also be used to mimic the cell bilayer. This has given rise to the study of antimicrobial peptides and how they interact with cell membranes. To characterize the pore formation of antimicrobial peptides as well as the ion flow, electrochemistry can be utilized. The ion flow created from the pore formation can be measured. It was first discovered in 1962 by Mueller et.al. when painting lipids that were suspended in organic solvents over a small hole in the microscale or nanoscale, the formation of black lipid membranes (BLM) occurs [3, 4]. However, there is a weakness in this approach. When painting the lipids, some of the organic solvents remain in the BLM which can denature proteins and destabilize the bilayer when the solvent evaporates. A solvent-free approach has been proposed, which is to deposit the bilayer directly on to the surface [3]. This can be accomplished by using liposomes.

Antimicrobial peptides (AMP) are a broad and unique class of biomolecules found in nearly all multicellular organisms. These peptides are part of the innate immunity of a wide range of species ranging from insects and amphibians to mammals [5]. The peptides can defend against pathogens ranging from bacterial infections, fungi, parasites and it has been reported that some AMPs are effective against tumour cells [5]. The field of investigating AMPs are growing rapidly as it has been reported that over 800 sequences for natural antimicrobial peptides and proteins [5] has been found and in 2014, 100 new peptides were found [5, 6]. The increasing prevalence of antibiotic resistance microorganisms means that new ways to combat these microorganisms are necessary [5, 6]. The main target of AMPs is the cell membrane of these pathogens [6]. Interactions between the AMPs and the cell membrane results in the formation of a pore membrane within the target cell membrane resulting in cell death. Due to this interaction, it is believed that pathogens may not easily develop resistance [5].

In this project the use of phospholipids, harvested from *E.coli* lipid membrane as well as lecithin from soyabean, to create nanopore-spanning lipid bilayer. These liposomes will

fuse on the surface of SiN_x nanopores and will be characterized with electrical conductivity by using Black lipid membrane (BLM) model. The coverage, as well as the morphology of the liposomes, will also be characterized The use of Antimicrobial peptides will be characterized on these model membranes if a successful layer has been established.

1.1 Membranes

In this section background information for the different membranes used in this project will be given.

The lipid membrane is a complex dynamic system of lipids called the fluid mosaic model. Lipids are composed of a hydrophilic head and a hydrophobic tail. Due to the hydrophobic tail, they will point inwards away from the aqueous medium and the hydrophilic head points outwards towards the aqueous medium. Membrane formation is due to the amphipathic nature of the molecules and it protects the cell from the extracellular environment and prevents molecules that are generated inside the cell from leaking out. The amphipathic nature of membrane lipids is the biggest distinction between the membrane lipids from other fatty lipids [7]. The formation of lipid bilayer is a self-assembly system meaning that the formation of lipid bilayers happens rapidly and spontaneously in water. [8] The fluidity of membranes depends on the acyl chains region comprising the hydrophobic domain of most membrane lipids [9]. Most lipid species in isolation can undergo a transition from very viscous gel (frozen) state to fluid (melted) liquid-crystal state as the temperature rises [7, 9].

The membrane is semi-permeable which means that only some molecules can diffuse through, like oxygen and carbon dioxide. Big molecules like water, ions and sugars cannot penetrate the membrane. [8] Different proteins can also be found on the membrane, called membrane proteins and these proteins are involved in the transport of solutes, signal transduction and anchoring of the cytoskeleton [8, 10]. These membrane proteins can span the membrane or are anchored on to the membrane from the outside to the inside. These membrane proteins have different functions, such as transport proteins which can transport ions e.g. H^+, K^+ and Na^+ which is vital for establishing the electrochemical gradients, which in turns drive other membrane transport processes on the cell [9]. A schematic of the mosaic model can be seen in figure 1.1.

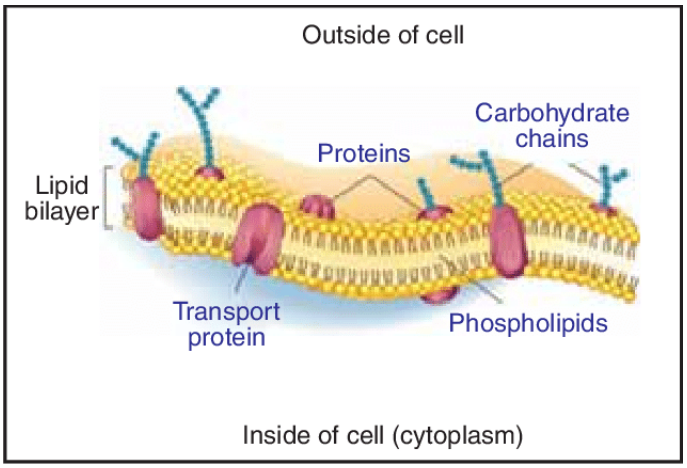

Figure 1.1: A schematic of the fluid mosaic model. Adopted from [11]

1.1.1 Phopsolipids

There are three classes of membrane lipids where the phospholipids are a major class. Phospholipids contain four components - two fatty acids attached to the glycerol backbone, and a phosphorylated group. The fatty acids constituent makes up the hydrophobic tail while the phosphate group is the hydrophilic head [8]. Depending on the hydrated phosphate headgroup, different phospholipids can be classified. In most eukaryotic membrane the most dominant phospholipids are observed to be phosphocholine (PC), phosphatidylethanolamine (PE), phosphatidylserine, phosphatidylinositol and cardiolipin [9]. For most prokaryotic membranes the major observed are phosphatidylethanolamine, phosphatidylglycerol (PG) and cardiolipin [9]. In figure 1.2 the major phospholipid classes can be seen [9].

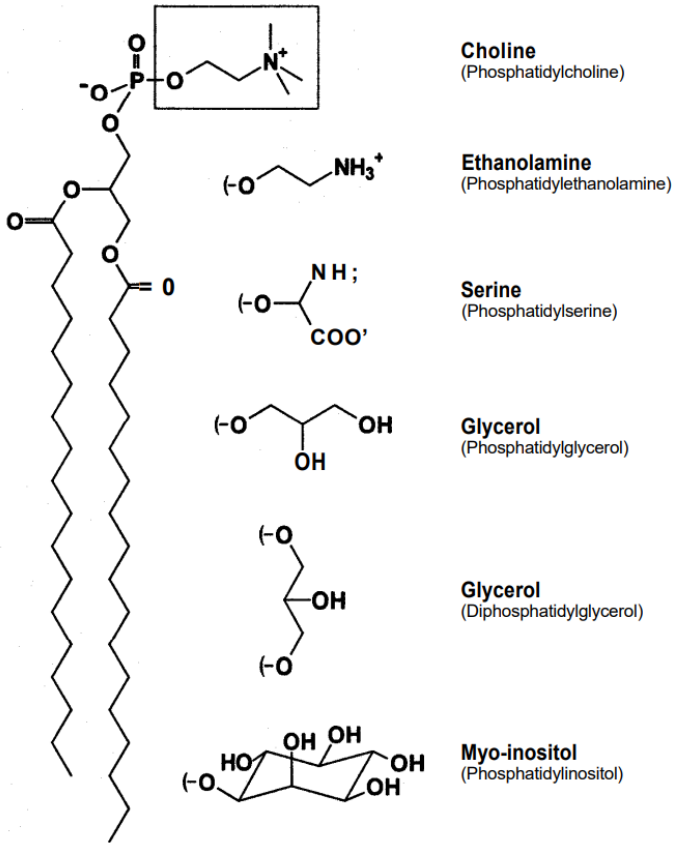

Figure 1.2: Composition of the phospholipids distearoylphosphatidylcholine. Headgroup for other major classes of phospholipids is also shown. Adopted from [9]

The composition of a cell membrane all have a different ratio of phospholipids and can vary drastically among different cell species. Different side of the membrane can contain different lipid species, as well as the symmetry of the bilayer. It is especially prevalent in terms of cholesterol content, which is another major class of the composition of a membrane [9]. It has been shown in *Erythrocyte* it contains mostly of cholesterol, PE and PC while cardiolipin was not observed. Cardiolipin is almost exclusively localized in the inner membrane of mitochondria suggesting that cardiolipin is required for the activity of cytochrome *c* oxidase [9, 12]. Mitochondria membrane also contains the highest amount of PE and PC compared to *Erythrocyte* [9].

1.1.2 Bacterial membrane

All bacterial organism has a cell membrane, which consists of lipids and a polymer called peptidoglycans. This polymer defines the shape of the organisms and is unique to prokaryotes. These polymers consist of a glycan backbone of muramic acids and glucosamine with cross-linked bridges for gram-positive organisms and partially cross-linked for gram-negative organisms. With gram-positive bacteria, the peptidoglycan is located on the outside of the organism and the lipid membrane is cross-linked under it

while gram-negative bacteria have two lipid membranes referred to as an outer membrane (OM) and an inner membrane (IM) [8]. These two layers of lipid membrane are separated by the peptidoglycan. In figure 1.3 a visual representation of the two types of bacteria membrane is shown.

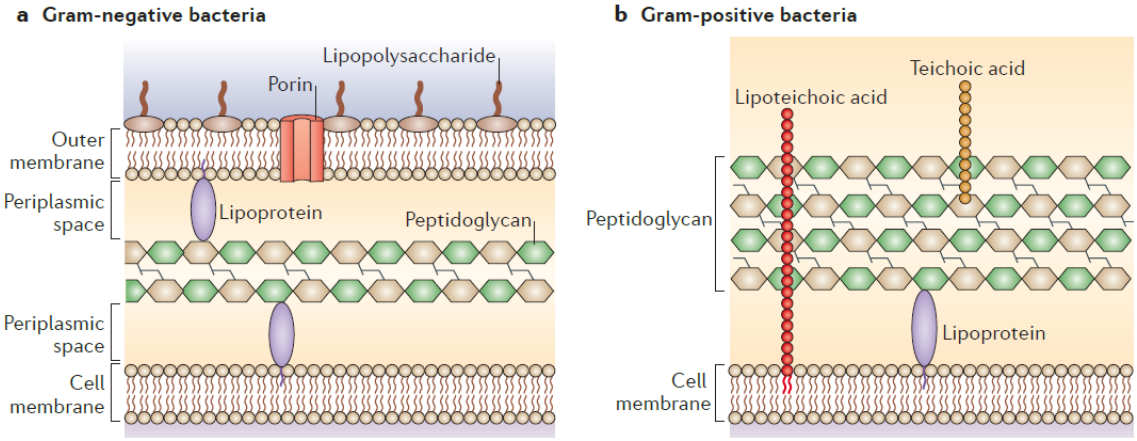

Figure 1.3: Schematic of the two types of bacteria. (a) Gram-negative bacteria. (b) Gram-positive bacteria. Adapted from Brown et.al. [13].

1.1.3 Saccharomyces Cerevisiae membrane

The *Saccharomyces Cerevisiae*, also called bakers yeast, is a eukaryote, single-celled organism and member of the fungus family. The outermost layer of the yeast cell is enveloped by a cell wall but is permeable by for solutes smaller than 600 kDa while also maintaining the structure and rigidity of the cell [10]. The plasma membrane forms a semipermeable barrier for hydrophilic molecules [10]. In contrast to bacteria in which the cytoplasmic membrane accommodates all membrane-associated processes yeast contains many specialized membranes [10]. There is also the plasma membrane which separates the other membranes and cell components from the external medium, the mitochondrial membrane, the endoplasmatic reticulum and Golgi apparatus, the nuclear membrane, the vacuolar and peroxisomal membranes [10].

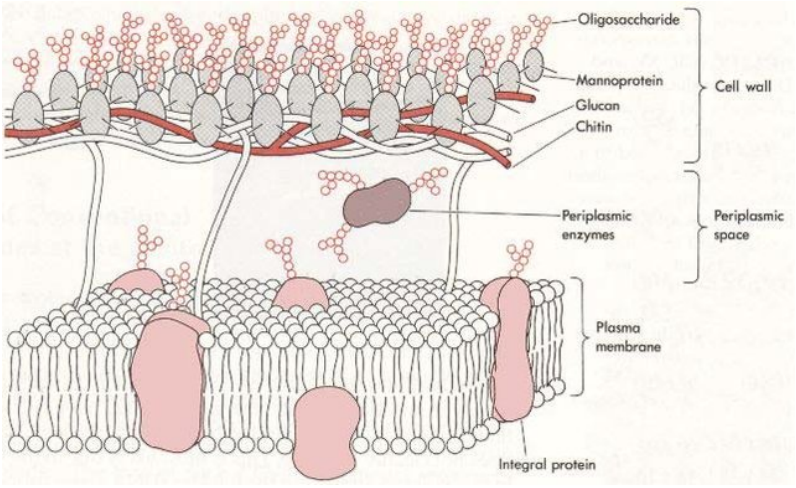

Figure 1.4: Schamatic of Saccaromyces Cerevisiae cell wall. Adapted from Marquina et.al. [14].

1.2 Amphapilic structures - lipids in water

The term surfactant comes from the words surface active agent. Due to their amphiphilic structure, they can be adsorbed at the air-water interface where the polar hydrophobic part point towards air while the non-polar hydrophilic part points towards water [15]. An interface is an area where two phases separate the boundary between them. Different interfaces exist as long as the two phases are of different forms e.g. gas/liquid, solid/liquid and gas/solid interfaces [15]. On an air/water interface the orientation of the surfactant would have hydrophobic tail point towards the air while the hydrophilic head will be in water [15]. Due to this adsorption, the surfactants change the surface properties. An example of a surfactant is soap, detergent, and lipids. Surfactants can be categorized according to the charge of their non-polar head, i.e. if the non-polar head is negatively charged is an anionic surfactant.

Surfactants and amphiphilic block copolymers assemble at low solvent concentration, forming the simplest amphiphilic structure called micelles [15, 16]. The reason for this assembly is because the surfactant wants to separate the contact between the non-polar solvent with the polar-solution. For example, when mixing water, oil and surfactant, the surfactant rests at the water-oil interface and this system is called emulsion and microemulsion [15]. The principle applies to both of them as the surfactant try to form an interface to separate the polar surface from making contact with the non-polar surface. Microemulsion system refers to the formation of micelles [15]. The form they make is either a spherical structure or a cylindrical structure. There are two types of micelles depending on the interface of the solvent called micelle and reverse micelle. Micelle structure is when the hydrophobic tail point in outwards and the hydrophilic heads are in the direction of the water. Reverse micelle as the name suggests is when the hydrophobic tails point towards itself and the hydrophilic head is outwards towards the water [15]. One can imagine that micelles are a droplet of oil in water, while a reverse micelle is a droplet of water in oil [15].

The formation of micelles only happens when it is above a specific concentration, called critical micelle concentration (CMC). In essence, the CMC is obtained when the interface has been saturated with surfactant and micelles are spontaneously formed [17]. The CMC can be seen as the surface tension as the function of concentration and is plotted on a logarithm scale. The formation of micelle as the CMC changes can be seen in figure 1.5.

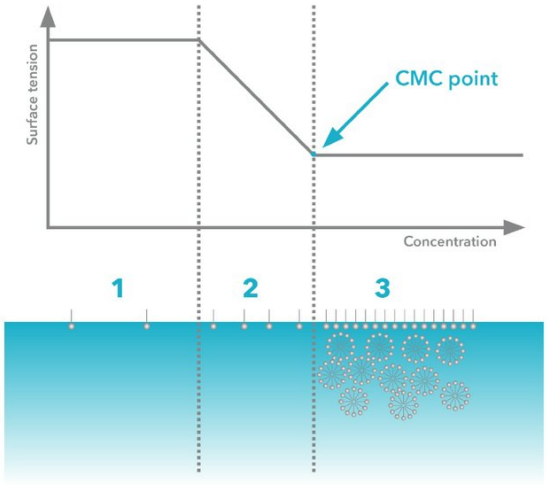

Figure 1.5: Schematic of the formation of micelles as the surface tension decreases and the concentration of surfactants increase. Adapted from McGiffen et.al. [18].

1.2.1 Vesicles

As mentioned previously surfactants and amphiphilic structures can form into micelles structures when the CMC has been reached. On the other hand, lipids usually form lamellar bilayer structures over the majority of their phase diagram, and in a dilute form, they form vesicles [16, 19]. Due to the lipid having two alkyl chains as the hydrophobic tail micelle formation are unfavourable relative to a bilayer structure. In solution, these lipids can either span out and make a planar lipid bilayer or a liposome. Liposomes and vesicles are the same thing and are used interchangeably [16].

When producing vesicles from lipids, one would have to evaporate the organic solvent from the lipids, either by rotary evaporation or air dry the lipid solution or by freeze-drying. This leaves a thin lipid film (if evaporated) which is then rehydrated by a polar solvent and vortexed. This produces a multilamellar vesicle (MLV) which as the name suggests is a vesicle/liposome with multiple layers surrounding each other as seen in figure 1.6(a). To get a unilamellar vesicle (ULV) the MLV have to be extruded with an appropriate membrane size, a ULV is then obtained. See figure 1.6(b) for the schematic of a ULV.

Due to the amphipathic nature of micelles as well as vesicles, they are used in the study of drug delivery systems for several years [9, 21, 22]. One of the obstacles in drug delivery is

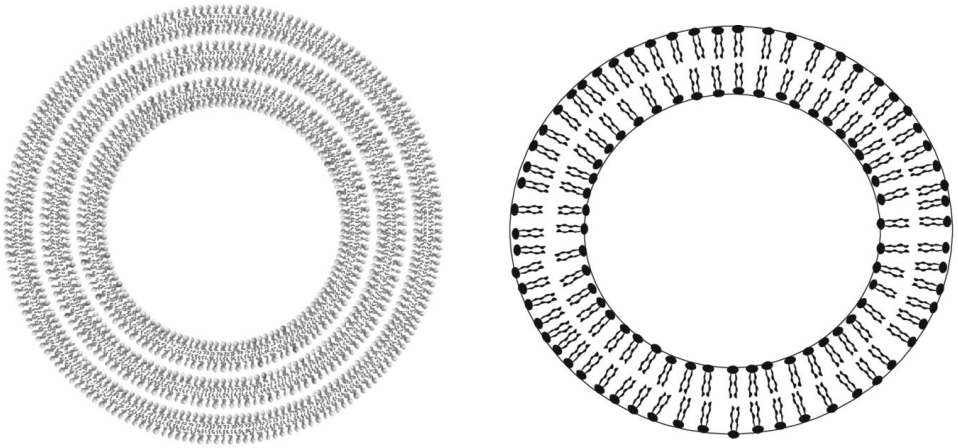

(a) A multilammelar Vesicle. **(b)** An unilammelar vesicle.

Figure 1.6: Schematic of a vesicle. (a) Is an multilammelar vesicle, and (b) is a single unilammelar vesicle after extrusion. Adapted from Stuart and Boekema [20].

the stability of these systems. The micelles and vesicles have to be stable and intact before reaching the target cell [23, 24]. It has been shown that gastric acid and bile salts have a detrimental effect on non-modifed vesicles [24]. Bile salts disrupt the bilayer composed of lipids with lower phase temperature such as PC [24].

1.2.2 Packing parameter

Several parameters determine the shape and formation of vesicles, as vesicles can come in a variety of shapes. The formation of vesicles can be viewed as a two-step self-assembly process, in which the amphiphilic structures form the bilayer, which then closes to form a vesicle [16]. The factor that determines the shape of the vesicle is the size of the hydrophobic moiety relative to the hydrophilic part [16]. It determines the curvature of the hydrophobic-hydrophilic interface described by the mean curvature H and its Gaussian curvature K, which are given by the two radii R_1 and R_2.

The mean curvature H is given by

$$H = \frac{1}{2}\left(\frac{1}{R_1} + \frac{1}{R_2}\right) \tag{1.1}$$

and the Gaussian curvature K

$$K = \frac{1}{R_1 R_2} \tag{1.2}$$

Thus the curvature is related to the surfactant packing parameter by this equation [16]

$$\frac{v}{al} = 1 + Hl + \frac{Kl^2}{3} \tag{1.3}$$

where v is the hydrophobic volume of the amphiphile, a is the interfacial area and l is the chain length normal to the interface. A schematic with the parameter is shown in figure 1.7.

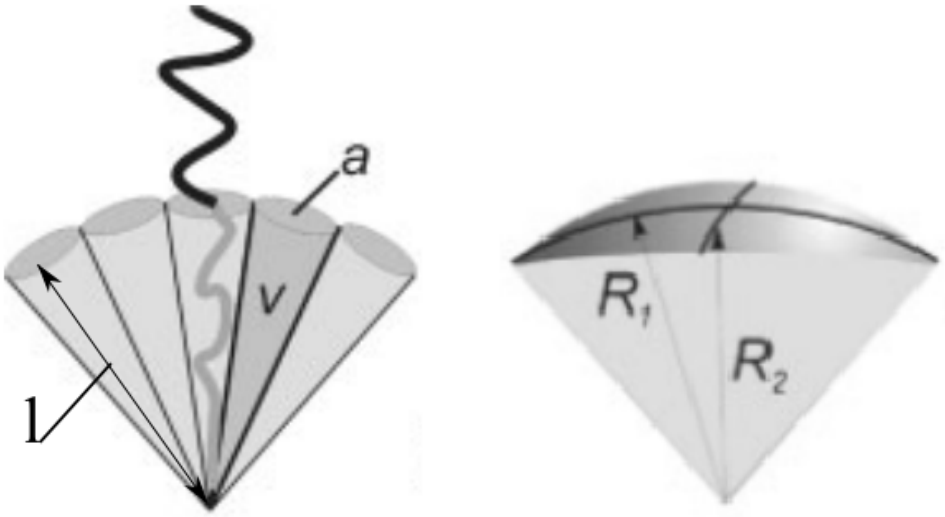

(a) Packing parameter **(b)** Curvature

Figure 1.7: Schematic of the packing parameter (a) and the curvature (b). The relation between the packing order and the curvature is given in the text. Adapted from Antonietti and Förster [16].

For phospholipid, with their double alkyl tail, they have a packing order of 1/2 - 1 and thus makes a spherical vesicle, and if the packing order is 1 then they make planar bilayers [20]. A list of different shapes at different packing orders can be seen in figure 1.8.

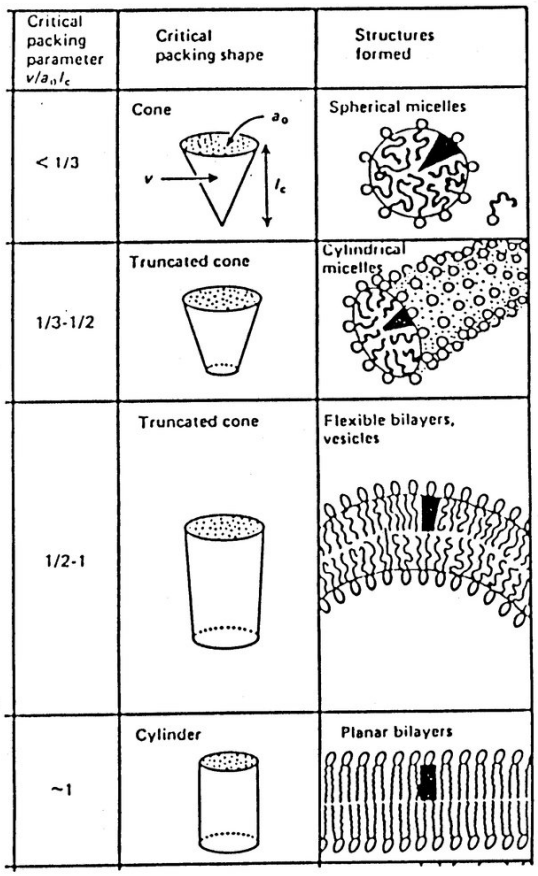

Figure 1.8: Different shapes at different packing orders. Adapted from Goyal and Aswal [25].

1.3 Model membrane systems

Due to the physical properties and functional role of individual lipid spices, it is difficult to ascertain in an intact biological membrane [9, 26].To study the biological membrane it is necessary to construct a model membrane. Thus, when making a model membrane three steps are required

- Isolation or chemical synthesis of a given lipid.
- Construction of an appropriate model system that contains the lipid.
- Incorporation of protein if desired.

The advantages of using a model membrane to study the membrane, the studies of biological membranes can be achieved in which the properties of individual lipid can be well-characterized [9, 26]. For liposomes specifically, the simplest form is the multi-lamellar vesicles (MLV) and is also the system that has been used for many years, but their use is only restricted to physical studies on bilayer organization [9, 26]. This restriction is due to the fact that only 10% of the total lipids of MLV is contained on the outermost bilayer. Thus unilamellar, which is a single bilayer, is produced either directly or from MLVs [9]. An MLV and a unilamellar vesicle can be seen in figure 1.6. Small unilamellar vesicles

(SUVs) can be produced from MLV by extruding the MLV through a french press, or by ultrasonic sound. The size of an SUV is in the range of 25-40 nm. Due to the size, it is not a favourable model for physical properties measurement on membrane lipids [9], as well, as the amount of aqueous buffer within the SUV membrane is often small which limits the studies that can be done. Studies such as permeability or ion distribution between internal and external compartments [9]. A better system would be the large unilamellar vesicles which are the same as an SUV, but with a larger diameter. The diameter of a LUV is shown to be in the range of 50-500 nm, and can also be produced by the same procedure as SUV [9].

Other systems include planar mono- and bilayers, as well as supported lipid bilayer [26].

1.3.1 Black lipid membrane

Black lipid membrane (BLM) referrers to a planar bilayer and are formed by dissolving phospholipid in an organic solvent and painting them across a small aperture [9, 27]. The reason that it is called black lipid bilayer is because of the lipids starting to form a thin film over the interface of the aqueous surface, and the lipids optical properties give it a black colour[9, 28]. The reason for this black colour is due to the reflected light on the water/lipid interface and a 180°phase shift at the lipid/water interface. This creates a destructive interference which gives this black colour [27, 28]. Using BLM model membrane one can measure the electrical properties of the barrier by using electrode in a two buffered chamber [9]. This technique allows ion channels and voltage-dependent ion fluxes to be measured. The lipids can span on an aperture that is on the microscopic level to millimetres [27]. As these lipids can span over these large diameters they are very fragile. The tension on these lipid spanning membrane is difficult to control - too little tension can cause fluctuation during measurements while a larger tension e.g. from the hydrodynamic pressure can cause the lipid membrane to break [27].

Preparation of BLM can be done in two ways. The originally, called solvent containing membrane and solvent-free membrane [27, 29]. In the case of solvent containing membrane, it is a simple method where the phospholipids self-assemble into a bilayer. The organic solvent, still trapped in between the bilayer, gets pushed to the edge of the aperture [9]. The bilayer formation is driven by mainly two forces - Laplace pressure and van der Waals force [28]. The hydrophobicity of the substrate induces a curvature within the lipid solution which in turns induces a pressure difference ΔP - that is the difference between P_{out} and P_{in} (figure 1.9(a)). This pressure difference is related to the radius of the curvature, R, and the interfacial tension γ [28].

$$\Delta P = 2\gamma/R \tag{1.4}$$

This pressure drives the monomeric layers closer to each other - which in turns drives the

organic solvent to the edge of the aperture. This phenomenon is referred to as membrane thining as the overall thickness of the bilayer reduces. Due to the van der Waal forces the "zipping" effect occurs (figure 1.9(b)), which results in the hydrophobic tails interact with each other and forms the overall bilayer structure (figure 1.9(c)) [28].

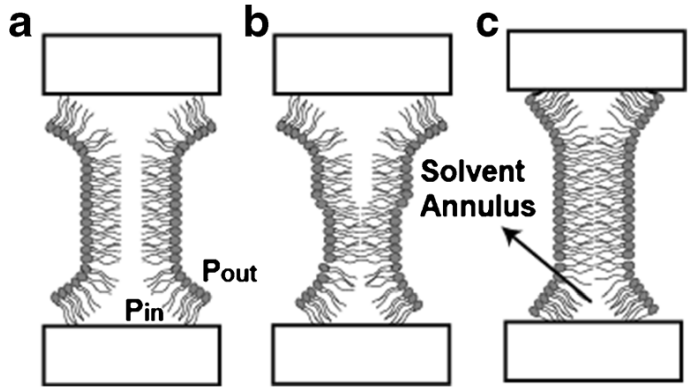

Figure 1.9: Formation of black lipid bilayer. (a) As the lipid as painted on the apparatus the pressure difference drives the two monomeric layers closer together, pushing the organic solvent to the edge. (b) van der Waals interactions between the two layers induce a "zipping" effect. (c) The final stage where the BLM is stable. Adopted from Bello et.al. [28].

1.3.2 Supported model membrane

Supported model membrane refers to the deposition of lipid bilayer of solid surfaces. These supported model membranes include supported lipid bilayer (SLB), polymere cushioned bilayer, hybrid bilayers and tethered bilayers [26, 30].

Different preparation approaches have been developed and the foremost methods are Langmuir-blodget(L-B)/Langmuir-Schaeffer (L-S) deposition, vesicle spreading and spin coating [31]. By spreading a monolayer of phospholipid on a subphase in a Langmuir trough the monolayer can be deposited on a substrate by pulling it through the air/water interface from the aqueous buffer. A second layer can be made by dipping the substrate, coated with monolayer, through the air/water interface again, from air to water [31, 32]. A schematic representation of the L-B/L-S deposition can be seen in figure 1.10.

The advantages with Langmuir-blodget/Langmuir Schaeffer deposition is the fact that you can control both sides of the bilayer, in terms of lipid composition resulting in greater control of assymetrical lipid composition [31, 32].

Using the method, vesicle spreading, to prepare supported lipid bilayer is by adding a droplet to the substrate [32]. After adsorption of the vesicles on the substrate, they spontaneously form a bilayer. Then excess buffer is washed away leaving symmetric bilayer [32].

After preparations, there are 3 main supported lipid bilayer, namely solid-supported lipid bilayers, tethered supported lipid bilayer and polymer cushioned lipid bilayer.

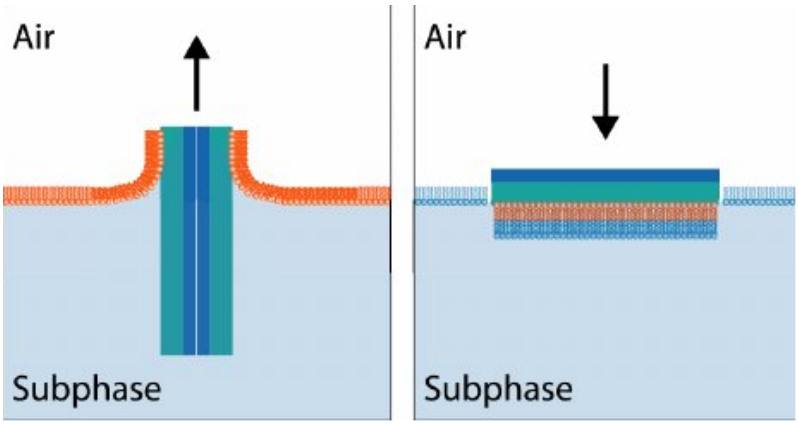

Figure 1.10: A schematic representation of a Langmuir-blodget/Langmuir-Schaeffer deposition. Left figure: The trough is getting pulled from the air/water interface, from buffer to air. Lipid monolayers will be deposited on the substrate. Right figure: The substrate is then dipped from air to buffer resulting in lipid bilayer. Adopted from Prudovsky et.al. [33]

Solid supported lipid bilayers consist of a lipid bilayer deposited directly on the substrate, and in the most simple form the lipids are in contact with the solid substrate - the only separation between the substrate and the lipid bilayer is a thin film of water [31]. Thus when making supported lipid bilayers an important factor to consider is the surface of the substrate. A clean hydrophilic surface is preferred and this is why mica, oxidized silicon and borosilicate glass is among the favoured substrate to use [26, 31]. A schematic representation of a solid-supported lipid bilayer can be seen in figure 1.11(a).

An alternative approach to solid-supported lipid bilayer is the so-called tethered lipid bilayer [31]. These tethered supported bilayers have a high electrical resistance and high long term stability [31]. Tethered supported bilayer works as an anchor and spacer to the bilayer where the inner leaflet is separated by this anchor [31]. For gold substrate, the use of thiol as an anchor has been used but for silicon surfaces the use of silane chemistry [31]. A schematic representation of a tethered supported bilayer can be seen in figure 1.11(b).

The third model supported model membrane is the so-called polymer cushioned bilayer. This was done to minimize contact from the substrate to the lipid bilayer. These hydrophilic polymers are usually bound to the substrate, and by chemi- or physisorbtion, and if designed appropriately mimic a cytoskeleton [31]. A schematic representation of a polymer cushioned bilayer can be seen in figure 1.11(c).

1.3.3 Using electroanalytical method to analyse the formation of lipid bilayer

Electrochemical methods have been used in many fields, one of these fields is the investigation of the formation of lipid bilayers [30]. It is known that biological membrane has electrical properties - they have a high electrical resistance for their thickness and a high capacitance [30]. With electrochemical impedance spectroscopy, the tiniest change on

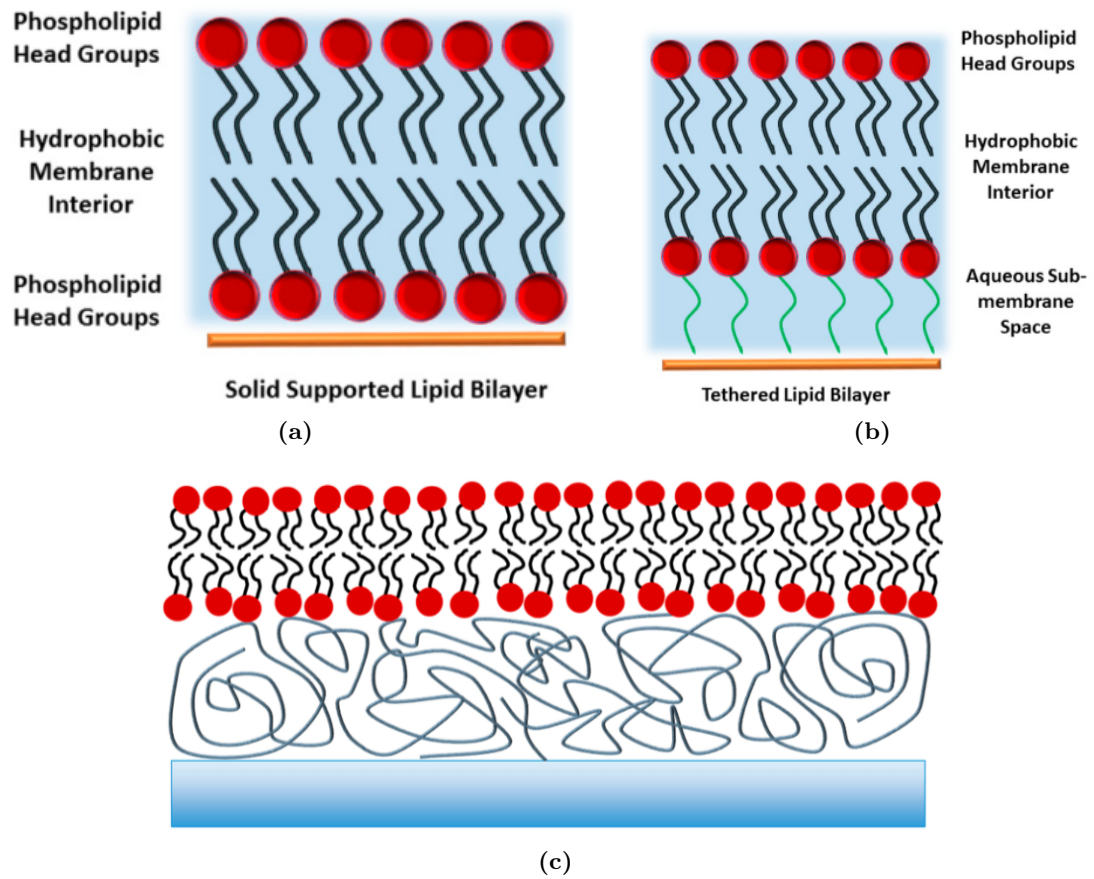

Figure 1.11: (a) Solid suported bilayer. (b) Tethered lipid bilayer. (c) Polymer cushioned bilayer. Adopted from Andersson and Köper [31].

the bilayer membrane can be measured. The electrochemical impedance measurement can be set up as an RC-circuit where the capacitance of the bilayer (C_{BLM} can be calculated as well as the resistance [30].

The contribution from the chip capacitance C is often ignored because the value is small.

The instantaneous current i can be calculated as

$$i = \frac{V}{R} + C\frac{dV}{dt} \tag{1.5}$$

From equation 1.5 it can be seen that if no formation of bilayer then the capacitance will not influence the instantaneous current. As soon as the formation occurs then the current will drop significantly.

The capacitance value is perhaps the most important value during this experiment as it directly related to the thickness of the membrane and the composition of the lipid.

The specific capacitance decreases linearly with an increasing amount of carbon atom in the fatty acid chain [30]. The thickness of the membrane can be calculated shown in

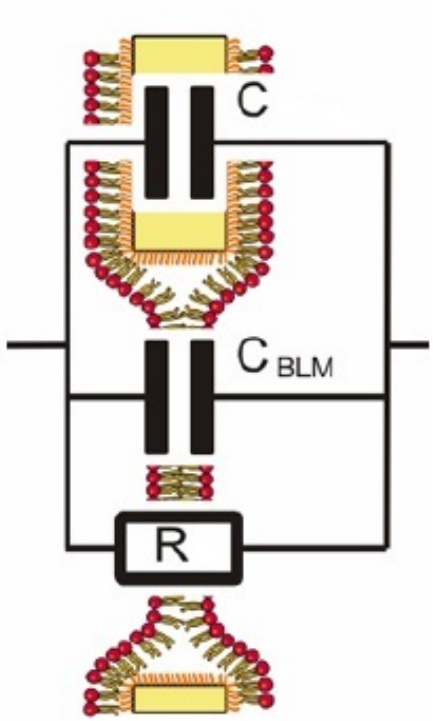

Figure 1.12: Schematic shows the RC-circuit with the capacitance from the lipid bilayer. Adopted from Studer [30]

equation 1.6.

$$C = \frac{\epsilon_0 \epsilon_r \cdot A}{d} \tag{1.6}$$

Where ϵ_0 is the permativity of free space, ϵ_r is the dielectric constant, A is the area of the aparatus and d is the distance between the two monolayers [30].

1.4 Anti microbial peptides

Antimicrobial peptides (AMPs) are an important component for animals as well as plant cell to defence against pathogenic microorganisms[34]. AMPs are always getting discovered and since 2014 more than 100 new AMPs have been registered in the antimicrobial peptide database increasing the total number of entries to 2493 [6].

These peptides are usually composed of 12-45 amino acids residues and AMPs have four features to defend against pathogenic microorganisms [34].

1. Selective toxicity - The peptide can distinguish between host cell and microbial cells.
2. Fast killing - The bacterial kill should be shorter than the targeted cell doubling time.
3. Broad antimicrobial spectra - One peptide should be able to target many species of microorganisms.

4. No resistance development - The peptide should have a mechanism such as the target microorganism cannot develop resistance against it.

1.4.1 Interaction between AMP and membrane

To fulfil these requirements must AMPs act on the cytoplasmic membrane of microorganism. The peptide utilizes a peptide-lipid interaction to permeabilize the target membrane [34] though there are AMPs that exhibit other forms of mechanisms other than membrane permeabilization [34, 35]. The peptide that acts on the membranes is mostly cationic due to the presence of Lys and Arg residues and forms amphipathic secondary structures (α-helices or β-barrels)[34], while anionic peptides are known most of the natural occurring AMPs are cationic with a net charge of +3.2 [6]. How these peptides damage the membrane are still debatable but three mechanisms have been proposed called barrel-stave-, carpet- and toroidal-model [34, 36]. Before the AMPs attach to the membrane they need to be attracted to the membrane surface first. The attraction mechanism between the peptide and membrane is electrostatic bonding between anionic and cationic peptides with the structures of the bacteria membrane [36]. For model membrane, studies have shown that AMPs penetrate monolayers, large unilamellar vesicles and liposomes containing acidic phospholipids [36]. However gram-negative and gram-positive bacteria are much more complex by nature than model membranes and cationic peptides are likely to attract to the negatively charges that exist on the outer envelope of gram-negative bacteria. Specifically, the peptides are attracted to the anionic phospholipids and phosphate groups on lipopolysaccharide (LPS) on gram-negative cells, and the teichoic acids on gram-positive cells. [36]. Figure 1.3(a) shows the schematic of the two types of cells. Once the peptide is close they have to transverse the capsular polysaccharide, which contains LPS for gram-negative cells and teichoic acids and lipoteichoic acids for gram-positive cells [36]. At low peptide/lipid ratio the AMPs are embedded parallel on the surface of the membrane and remains inactive. As concentration rises the orientation changes from parallel to perpendicular and the AMPs starts to insert into the membrane forming transmembrane pores.

1.4.2 Barrel-stave model

In this model, the peptides form barrel-like pores with the staves being individual peptides protruding the membrane perpendicularly. The hydrophobic region of the peptides faces the hydrophobic membrane core, while the hydrophilic regions form the pore lining (figure 1.13(a)). [36]

1.4.3 Carpet model

The carpet models describe AMPs that accumulate on the surface of the membrane, covering it due to electrostatic interactions with the polar head groups, as all AMPs due.

In this model, the case of a high concentration of peptides is considered. Due to the high concentration of peptides the surface of the membrane is disrupted, instead of forming pores. This disruption will lead to the formation of micelles (figure 1.13(b)). [36]

1.4.4 Toroidal model

In this model, the peptides form pores similar to the barrel-stave model, but instead of penetrating the membrane the peptides associated with the lipid heads and bend the membrane to form pores. This creates a membrane pore that is intercalated with the membrane lipids (figure 1.13(c)) [36].

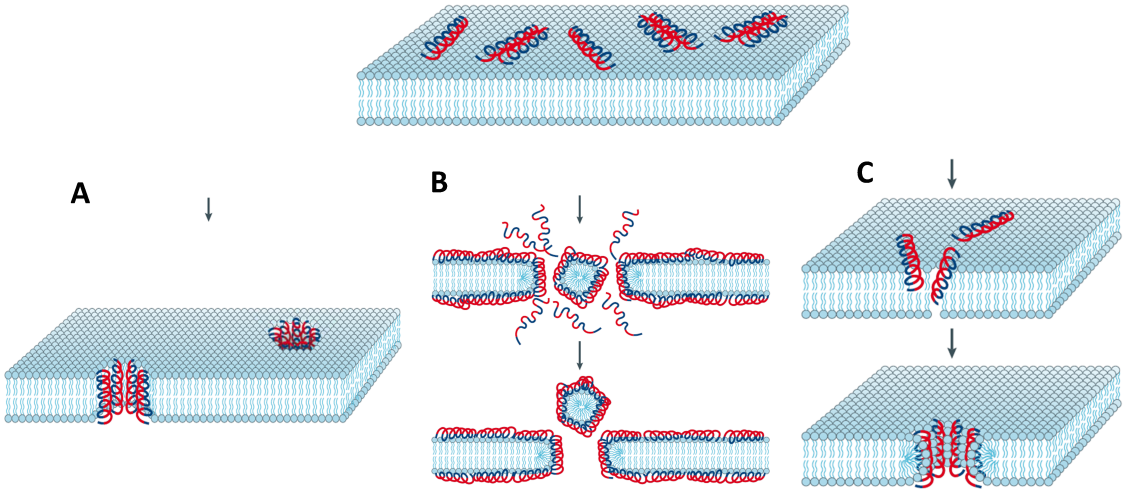

Figure 1.13: A visual representation of the three models. (a) Barrel-stave model. (b) Carpet model. (c) Toroidal model. Adapted from Brogden [36].

1.4.5 Structure parameter

One thing that AMPs have in common is that they possess amphipathic features, that allows them to interact with membranes [37]. Though other structural parameters for AMPs can be used to describe the peptides, their antimicrobial activity and selective toxicity. These parameters are interdependent, which means that one change in one parameter will likely results in a change in another parameter [37]. These parameters are conformation, charge, hydrophobicity and polar angle.

1.4.6 Conformation

AMPs can be divided based on their three-dimensional structures as most are either α-helical or β-sheet peptides [37], while the rest can mostly be classified as peptides enriched in one or two amino acid residues.

1.4.7 Charge

As mentioned before most cationic AMP has a net charge of +3.2. In general, an increase in AMP charge the more activity the peptide has, but having too high charge can also reduce the activity [6, 37].

1.4.8 Amphipathicity

One of the main features of AMP is their amphipathicity. The simplest form is created by a simple α-helix and due to the periodicity, all of the hydrophobic residues can be located on one side of the helix [37]. Thus two characteristics were used to describe amphipathicity: Hydrophobic moment and linear hydrophobic moment [38].

1.4.9 Hydrophobicity

The overall hydrophobicity of AMPs are defined as the sum of energy transfer of the residue (transfer of energy into a hydrophobic environment) [38]. Too high hydrophobicity loss of antimicrobial activity is observed - generally, AMPs have a hydrophobicity of 50% [37, 38].

1.4.10 Selective toxicity

As mentioned before cationic AMPs target specific structures on the membrane. This is the reason why AMPs can be toxic to specific cells. Furthermore, the composition of bacterial cells consists of large amounts of negatively charged phospholipids, phosphatidylglycerol and cardiolipin. This results in a higher affinity to bacterial cells. Compare this composition with mammalian cells where the surface is electrostatic neutral and made exclusively of zwitterionic phospholipids, mainly phosphatidylcholine and sphingomyelin as well as cholesterol which has shown to protect the membrane from anionic AMPs [34]. Figure 1.14 shows a schematic of the affinity for an AMP.

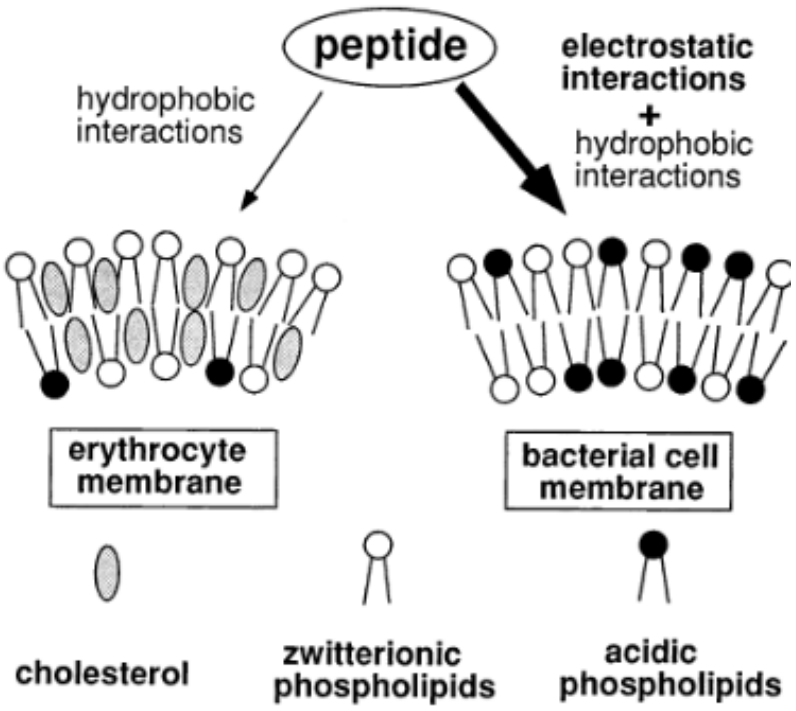

Figure 1.14: Schematic showing the affinity of AMP. With mammalian cells peptide has a less affinity to (right side) as it mostly contains zwitterionic phospholipids. While bacterial cells contains acidic phospholipids which increases the affinity. Adapted from Matsazuki [34].

1.5 Dynamic light scattering and nano tracking analysis

Dynamic light scattering (DLS) is a method that can determine the size, size distribution and shape of a particle suspended in solution through Brownian motion and Doppler shift induced by a laser [39]. When particles are moving in suspension the Brownian motion is excited by a monochromatic laser, the wavelength of the incoming light changes after hitting the particles which in turn creates a Doppler shift. The result of this Doppler shift means that the frequency of the scattered light is different from the unscattered light [39]. The correlation between the size distribution and the motion of the particles can be obtained by using an autocorrelation function and measuring the diffusion coefficient of the particles [39]. The use of an autocorrelation function is to allow the analysis of time-dependent fluctuations in the intensity of the scattered light and the diffusion coefficient D is related to the hydrodynamic diameter D_H derived by the Einstein-Stokes equation [39]. The hydrodynamic diameter represents the diameter of a hypothetical hard sphere that has the same diffusion coefficient as the physical particle under investigation [39]. In figure 1.15 is a schematic of the hydrodynamic diameter.

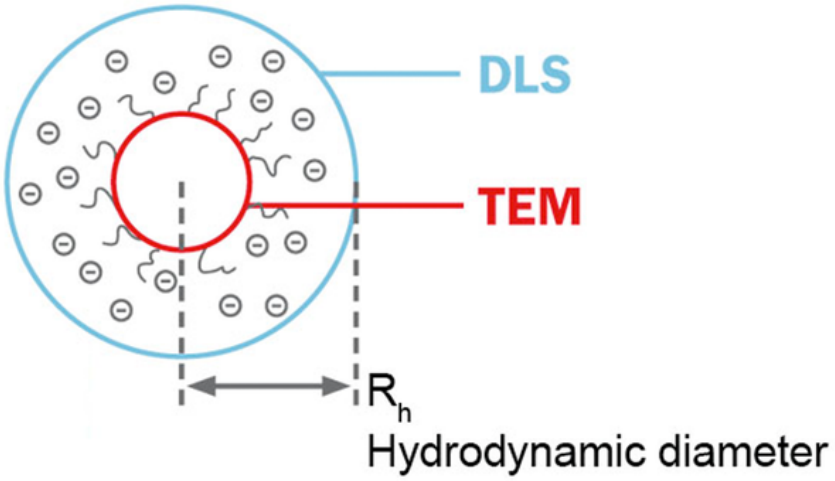

Figure 1.15: Schematic of the hydrodynamic diamter. Adapted from Crolly [40].

The relationship between the diffusion coefficient and the hydrophobic diameter is given by the Einstein-Stokes equation

$$D = \frac{k_B T}{6\pi\eta r} \tag{1.7}$$

where k_B is the Boltzmann constant, T is the temperature, η is the viscosity and r is the radius. Rearranging for r gives the hydrodynamic radius.

$$r = R_H = \frac{k_B T}{6\pi\eta D} \tag{1.8}$$

The hydrodynamic diameter for a sphere is therefore

$$D_H = \frac{k_B T}{3\pi\eta D} \tag{1.9}$$

The exponential decay rate of the correlation of the signal G is also dependent on the diffusion of the particles and is given by

$$G = B + Ae^{-2q^{2D\tau}} \tag{1.10}$$

where B is the baseline, A is the amplitude, D is the diffusion coefficient. The scattering vector (q) is given by

$$q = \frac{4\pi n}{\lambda_0} sin\left(\frac{\theta}{2}\right) \tag{1.11}$$

A schematic overview of a DLS setup is shown in figure 1.16

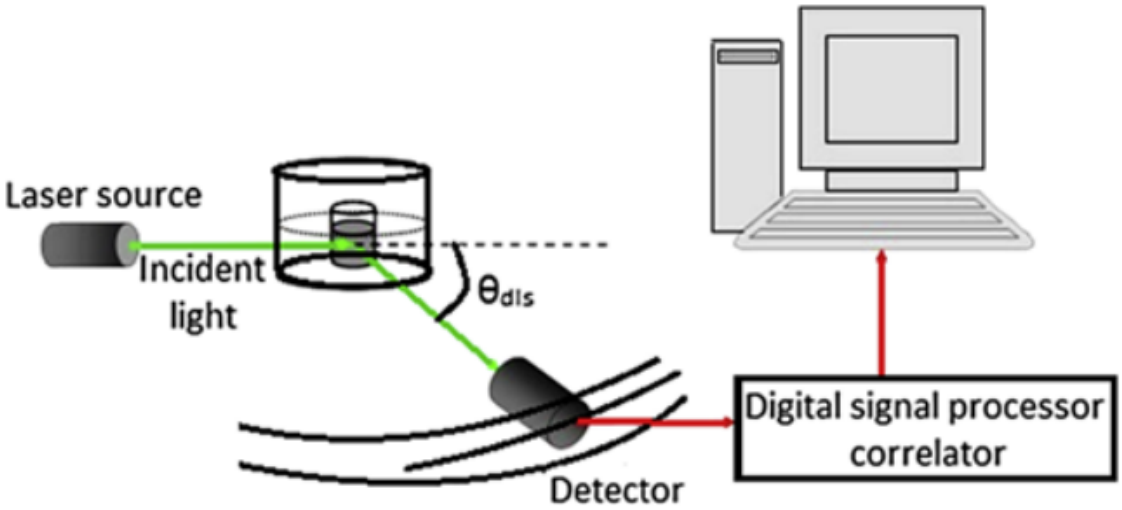

Figure 1.16: Schematic overview of a dynamic light scattering setup. Adapted from Sakho et.al. [39].

1.6 Lithography

1.6.1 Pore milling

An important element in the production of nanopores is the high degree of control of the size of the nanopore. Being able to control the size ensures adequate sensitivity and reproducible of the nanopore. [41]

A method is called focus ion beam (FIB). To get a small pore size the ion beam must also have a small diameter at the point of contact with the silicon [41]. This is achieved by optimizing variables such as astigmatism and the magnification. The most widespread ion source is liquid metal ions, especially the use of gallium ions [42].

Focus ion beam in principle is derived from the sputtering mechanisms, which means that the atoms from the surface are ejected from the bulk [41, 42]. The sputtering yield is usually high when using 30keV Ga^+ ions. Sputtering yield refers to how many the ions can transfer its kinetic energy to the target atom and overcome the surface energy [41]. The interaction between the incident ion and the target atom can be modelled as an elastic two-body collision, the maximum transferable energy can be calculated as seen in equation [41].

$$E_{max} = \frac{4M_1M_2}{(M1M2)^2} \tag{1.12}$$

Materials and Methods 2

In this chapter the materials will be presented as well as the methods used in the project.

2.1 Materials

\textbf{Chemical}	\textbf{Lot no.}	\textbf{Manufacturer}
Agar	BCBP0217V	Sigma-Aldrich
Tryptone	HO170W	VWR Chemicals
APTMS	BCBV6395	Sigma-Aldrich
Chloroform	SHBJ2941	Sigma-Aldrich
Disodium phosphate	F1485086722	Merck
Ethanol 99.9	64-17-5	VWR
HEPES pH7	1121871	Fluka
KCl	1121871	Fluka
Monosodium phosphate	20k0228	Sigma-Aldrich
Methanol	SHBH9443	Sigma-Aldrich
Peptone	BCBN4114V	Sigma-Aldrich
Sarcosine	SLBV0716	Sigma-Aldrich
Sulphoric acid	SZBF3430V	Fluka
Toluen	STBH8620	Sigma-Aldrich
Yeast extract	813-d-2	Microbioligy Fermented
\textbf{Lipids}		
DPhPC	850356C-25mg-A-145	Avanti Lipids
Lecithin		Biosym

Table 2.1: The following table shows all the chemicals and lipids that were used in this project.

2.2 Methods

2.2.1 Purification of *Escherichia coli* outer membrane

E.coli BL21(DE3) was incubated overnight with an RPM of 180 at 37°C. They were grown to an optical density of $OD_[600]$ of 1.879. The cells were disrupted using a Dounce tissue grinder (Sorvall Lynx 4000). The crude extract was fractioned by centrifuge (Soval Lynx 4000) at 60,000 x g for 10 minutes at 4°C. The supernatant was discarded and the pellets containing the cells were resuspended with 10 mL 20mM sodium phosphate pH 7 and 2% N-lauroylsarcosine (Sigma) to solubilise the inner membrane. The pallets were solubilized for 1 hour with rolling. The extract was then centrifuged at 60,000 x g for 1 hour at

10°C. The supernatant was discarded and the pellet, enriched in outer membranes, was resuspended in phosphate buffer. Modified protocol from Beis et.al. [43].

2.2.2 Purification of *Escherichia coli* for liposome preperation

Total lipid extraction was done by centrifuging the liquid cell culture at 10,000 x g for 10 min at 4 °C in a teflon centrifuge tube. Then the pellets were suspended with milliQ-water and ran through the centrifuge again. They were then resuspended in with milliQ-water (5ml/g cell paste) and tip sonicated with 15 sec on/off for 5 minutes. 2.2 methanol and 1ml chloroform were added per 1ml aliquot. They were then centrifuged at 800 x g for 10 minutes at 4 °C. This induces a phase-separation where the lower phase is the chloroform with the lipids. This lower phase was carefully extracted out with a glass pipette and the upper aqueous phase was twice reextracted by addition of 1ml chloroform. Protocol from Lind et.al. [44]

2.2.3 Extraction of chloroplast from spinach

A couple of leaves were added to the mortar and liquid nitrogen was added to freeze the leaves. The leaves were grinded until they were a fine powder. The powder was mixed in a blue cap bottle with 30 mL citrate buffer pH 7. The extract was vortexed for 3 minutes and then filtered twice through a coffee filter. The insolubilized materials were separated by centrifuge at maximum speed for 10 minutes. The supernatant was discarded and the pellets were resuspended in citrate buffer and stored in the freezer. Modified protocol from Klinkenberg et.al. [45, 46].

2.2.4 Purification of *Saccharomyces cerevisiae* plasma membrane

Yeast cells were disrupted using a Dounce tissue grinder. The crude extract was fractioned by centrifuge (Sorvall Lynx 4000) at 60.000 x g for 30 min. The supernatants were discarded and the pellets were washed in dH_20 at the same settings. The supernatants were discarded and the pellets were resuspended with 1.5 ml dH_20 and mixed with 20 ml 1:17 methanol-chloroform mixture. The entire mixture was added in a separator and shaken and two phases were observed. The aqueous upper phase was rewashed with 1:17 methanol-chloroform buffer and the lower organic phase were stored. The upper phase was then rewashed twice in a 1:2 methanol-chloroform buffer. All the organic phases were then added in a round flask and were run through a rotary evaporator to evaporate the chloroform from the lipid. The lipid was then stored with 1:2 methanol-chloroform buffer in the freezer

2.2.5 Visualization of lipids with thin layer chromatography

The eluent was made by a chloroform-methanol-water buffer with the ratio of (65:25:4). 65 ml of chloroform was pipetted into a bluecap bottle. 25 ml of methanol was pipetted

into the mix and 4 ml of dH_20 was added. The entire pipetting process was performed in a fume hood. A 10 % sulphuric acid was made by mixing 10 ml sulphuric acid with 99.9 % ethanol. The eluent was added into the thin-layer chromatography (TLC) chamber and was left to equalize for 30 min. During those 30 mins. preparation of the TLC plates was done. With a pencil a horizontal line was made approximately 2 cm. from the bottom of the plate. 2 lanes, A and B, was marked. On lane, A 2 μL of sample solution containing the yeast lipid was added and on lane B 3 μL of material was added. After 30 min. the plates were inserted into the chamber, making sure the eluent does not make contact with the origin, but high enough to touch the silica gel plates. It takes approximately 30 min. for the eluent to travel up the silica plates, where it ends 1-2 cm from the top of the plate. After removing the plates from the TLC chamber the plates were left to air dry for 20 min. While airdrying a hot plate was turned on and set to 250°C. When the plate was dry a 10 % sulphuric acid was sprayed on the plate - making sure the entire plate is covered. The plate was then placed on the hotplate and the lipid will be visible as black/brown marks.

2.2.6 Liposome preparation

Lipids that were harvested from microorganism and dissolved in chloroform/methanol solution were dried under a stream of nitrogen. The resulting lipid film was then put in a vacuum desiccator overnight to fully evaporate the remaining solvent. The lipid film was then suspended in 5 ml TBS-buffer and hydrated for minimum 1 hour in a water bath at 50°C. Afterwards the sample was tip sonicated for 20 minutes with a 5 second pulse on/off and the sample was in an ice bath to prevent thermal degradation to the sample. Afterwards, the sample was extruded (Avanti mini-extruder) with 100nm polycarbonate membranes with sizes. The sample was passed through a filter 11 times. This will produce large unilamellar vesicles of sizes around 100nm. Protocol by Lind et.al. [44].

2.2.7 Dynamic light scattering

Dynamic light scattering (Zetasizer nano series) was used to measure the size of the produced vesicles. 1ml of sample was transferred to a cuvette. The cuvette was inserted into the machine and the relevant standard operating procedure (SOP), notably the dispersion is set to water, and temperature on 25°C.

2.2.8 Visualization with atomic force microscope

Visualization of chloroplast/liposomes was done by atomic force microscope (Multimode 8). Material was deposited on mica slides and left for 30 minutes to let it sit. Afterwards, the sample was rinsed with dH_2O to remove contaminants and excess buffer. The sample was then dried with oxygen to remove the rinsed dH_2O. The sample was then visualized with AFM. For visualization of nanopore arrays on silica nitride and silica oxide, 5 μL material was deposited. The imaging was done in tapping mode. The data was processed with Gwyddion (Ver. 2.53)

2.2.9 Visualization of with scanning electron microscope

Visualization of SiN_x nanopores was performed a Zeiss (Gemini 1540 xb) scanning electron microscope (SEM). The SiN_x substrate were attached to a SEM stage.

Drilling of nanopore arrays

Drilling of nanopore arrays was done with a focused ion beam (FIB) with Elphy plus (Raith). The dose was increased for every pore that was drilled starting with at 25 and increasing the dose with a value of 2 each time ending with 233.

2.2.10 Formation of lipid bilayers

Formation of lipid bilayers and electrochemical measurements were all performed by using a kit from Elements as well as from Nanopore. The experiments were done according to a protocol for lipid bilayer formation, provided by Elements. A short overview will be given below

Lipid bilayer kit

The kit used in this project was a combination of using the instruments from Elements and the nanopores from Nanopore. The instruments from Elements was an eONE-XV(S/N eONE0143) USB connected amplifier and the software elements data reader 3 (EDR3, version 0.7.0 for Windows). Membrane formation was monitored using protocol 1 and set to 100mV.

From the company, Nanopore solutions, SiN_x nanopores were obtained as well as a cassette made of teflon to hold the nanopores and an electrochemical flow cell chamber also made of teflon. Figure 2.1 shows an illustrations of the setup.

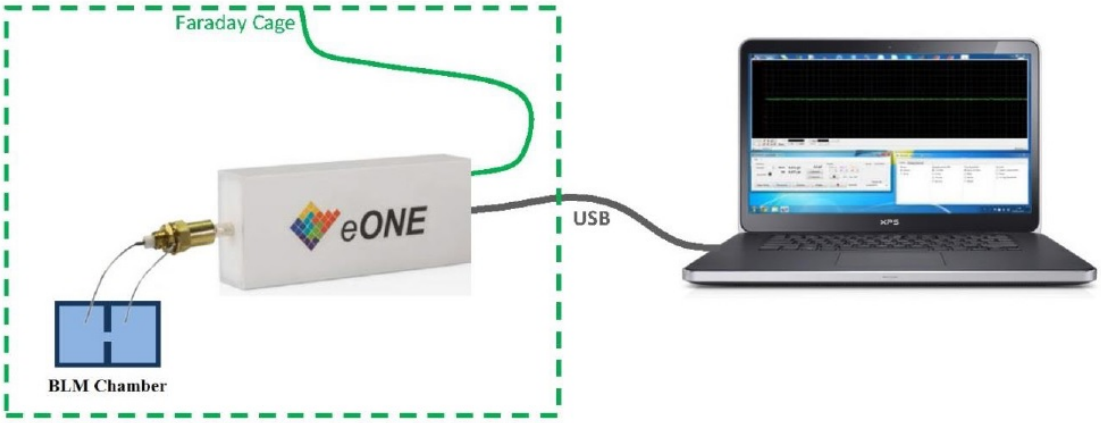

Figure 2.1: Illustrations of the setup used to measure the formation of lipid bilayeres.

Membrane formation

The lipid bilayer formation was formed by depositing 60μL liposomes onto the surface of the 60x30nm nanopores while already submerged in electrolyte (1M KCl, 10mM HEPES). After deposition self-assembly of bilayers should occur.

Electroplating of silverwires

Ag/AgCl wires were prepared by electroplating silver (Mateck, diameter=0.5mm Art. Nr. 901644-1) using cyclic voltammetry in a 1M KCl solution. This was done using Gamry Reference 600^TM instrument (Serial number 02039) with the Framework acquisition software (Version 7.04, build 4758) provided by Gamry. The electroplating was performed with platinum (Gamry #935-00056) counter electrode and a carbon reference electrode. Cyclic voltammetry was run twice to ensure proper coating with the parameters from table 2.2.

Parameter	Value
Scan limit 1	0.2V
Scan limit 2	-0.005V
Scan rate	50 mV/s
Step size	2
Cycles	10
Max current	50mA

Table 2.2: Cyclic voltammetry parameters

The Ag/AgCl wires were used within 2-3 days, before electroplating again. The used wires were cleaned before recoating by passing the wires through a flame to remove the layer of AgCl layer. The wires were then rubbed with extra fine sandpaper (#4000) until the surface was completely free of the AgCl layer. Finally, the wires were washed with water and 70% ethanol.

Funtionalization of SiN_x surface

Functionalization of SuN_x substrates was done by treating it with a UV-ozone by placing the SiN_x substrates in a UV-ozone chamber (Bioforce Nanosciences, pro cleaner) for 15 min. In the meantime, the APTMS solution was prepared by adding 750 μL toluene and 250 μL APTMS in an Eppendorf tube. After the substrates were treated with an ozone layer they were put into a vacuum desiccator with the APTMS solution. The desiccator was flushed three times, 10 minutes in between each flush, before letting the treatment of the substrate in vacuum for 1 hour.

Mounting the SiN_x substrate

When mounting the SiN_x substrate on to the cassette great care was needed due to the dimensions of the substrate. The cassette was disassembled and the substrate was put

in between two o-rings. When assembling the cassette due to the teflon material, it is important not too over tighten the bolts as it can damage the thread. When the substrate has been mounted the chip was wetted with 70% ethanol and pipetted up and down to remove any bubbles. This was done twice. Then the same procedure was done with milliQ-water. These two wetting procedures were done on both sides of the cassette.

Cleaning of mounted SiN_x substrate

The surface of the SiN_x substrates need to be as clean of contaminants as possible, the use of Piranha solution to clean the surface was used. Piranha solution is a strong oxidizing agent and contains concentrated sulphuric acid and 30% hydrogen peroxide in a 3:1 ratio. Piranha solution will remove most organic compounds therefore when handling piranha solution, great care must be taken. 15ml sulphuric acid was pipetted into a beaker then 5ml hydrogen peroxide was pipetted in the beaker creating 20ml of piranha solution. Then the entire cassette was placed in the beaker for 10 minutes occasionally stirring the cassette. Afterwards, the cassette was removed with steel tweezers and rinsed vigorously in milliQ-water and stored in a container with water. The entire cleaning procedure was done under a fume hood with two layers of nitrile gloves and eye protection.

The protocol for assembling of the electrochemical flow cell, as well as the cleaning protocol, was provided by Nanopore solutions.

Data processing

The recorded data were processed with MatLab (R2016a) using the provided MatLab script from Elements.

Results 3

In this section, the results will be presented.

3.1 Thin-layer chromatography

Thin-layer chromatography was performed to verify the presence of lipids after harvest of membrane lipids from *E.coli*. Lecithin was used as a control because of the abundance of lipid structure present.

Figure 3.1: Lecithin was used as a control for TLC measurements. Mobile phase was a solution of 65:25:10 chloroform/methanol/water. Spots can be observed. A destructive visualization method was employed with a 10% sulphoirc-ethanol

The mobile phase in use was a solution of 65:25:10 chloroform/methanol/water. In figure 3.1 the TLC measurement can be seen. The retention factor (R_f) values has been calculated for each spots in table 3.1.

		Distance moved (mm)		
Lane	Spots	By spots	By lane	R_f
A	Lecithin	51	82	0.622
		54	82	0.6
		59	82	0.720
		66	82	0.805

Table 3.1: Table of the R_f values for the difference spots.

(a) 65/25/10 mobile phase ratio.

(b) 65/25/10 mobile phase ratio.

(c) 65/25/10 mobile phase ratio.

(d) 75/25/10 mobile phases ratio.

(e) 85/25/10 mobile phase ratio.

Figure 3.2: (a-c) used the same mobile phase but no burn marks was observed on the lanes. (d-e) A different ratio was used. The amount of chloroform was increased in order to make the mobile phase more polar. It can be observed that the lane has not moved at all, indicating a too high polarity.

In figure 3.2(a-c) the TLC was performed with the same solution ratio as the lecithin but no bands were visible. Thus a ratio change in the mobile phase solution was done by increasing the polarity of the solution. This resulted in the spotted sample not moving at all as seen in figure 3.2(d-e).

3.1.1 TLC on *saccharomyces cerevisiae*

TLC was also performed on the yeast membranes. The same approach was done as with *E.coli* lipids.

(a) 65/25/10 mobile phase ratio.

(b) 80/15/4 mobile phase ratio.

(c) 80/15/4 mobile phase ratio.

Figure 3.3: (a) Two lanes of the same lipid solution was performed on lane A and B respectively. No bands can be. (b-c) Increased polarity of the mobile phase but no bands were observed.

It can be observed from figure 3.3, that no bands can be observed. This could indicate that no phospholipids were harvested from the *Saccharomyces cerevisiae* plasma membrane.

3.2 Dynamic light scattering

Dynamic light scattering (DLS) was performed to check for the size of the liposomes. The zeta potential (not shown) were also performed but due to low concentration, no graph was made. Though from the zeta potential measurements it was confirmed that the liposomes were negatively charged. The range for all the graphs is from 0.4nm - 10,000nm.

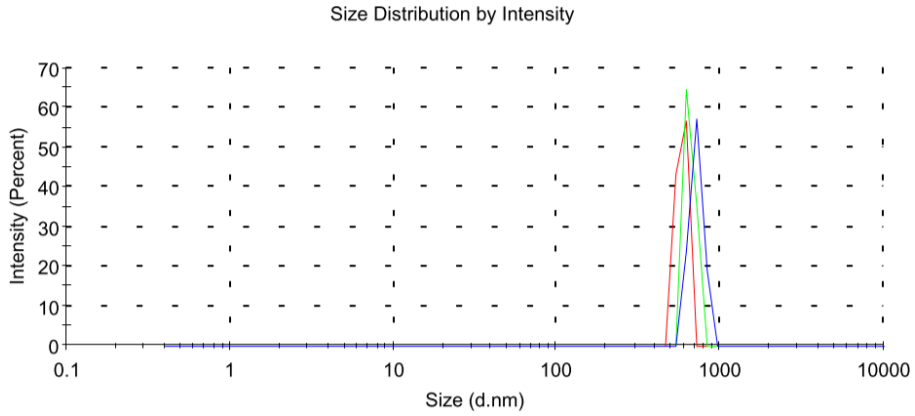

(a)

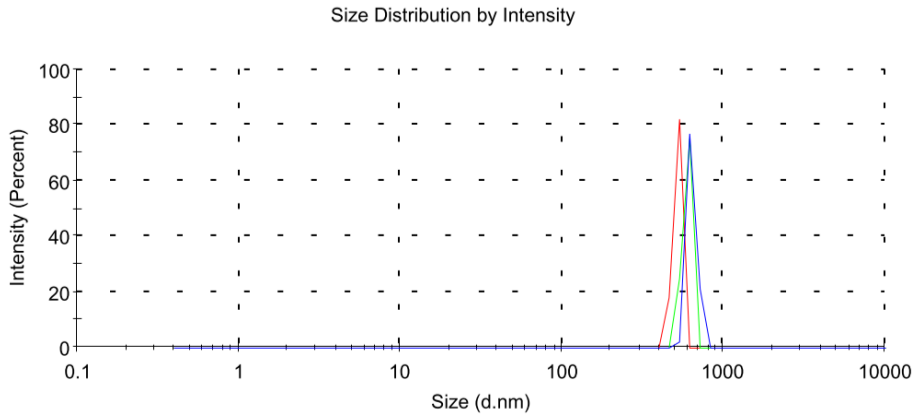

(b)

Figure 3.4: The first measurements with DLS shows a size of 710nm ± 68.23 and 518 ± 27.83 with a polydispersity of 0.598 and 0.794 for (a) and (b) respectively.

The liposomes from figure 3.4 did not yield the desired size as they were too big. This was because the liposomes did not undergo an extruding process yet.

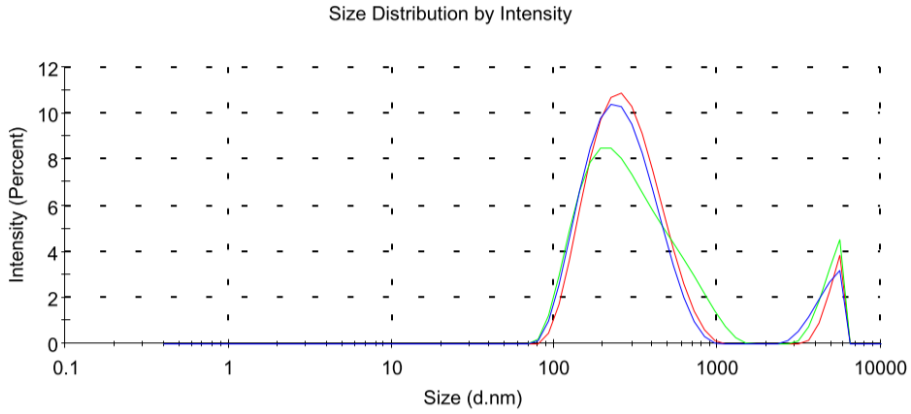

(a)

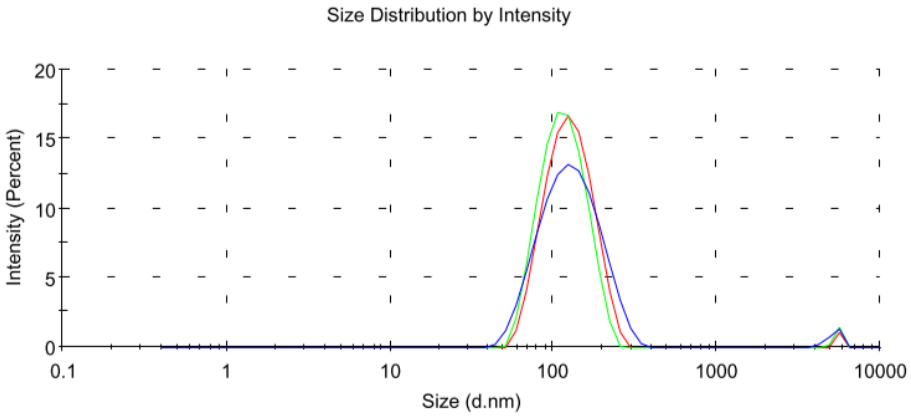

(b)

Figure 3.5: DLS measurements shows a size of 292nm ± 142.6 and 128nm ± 41.06 with a polydispersity of 0.340 and 0.336 for (a) and (b) respectively.

In figure 3.5 were samples that were extruded before measurement and gives the expected average size of 100nm, with a pdi of 0.340 and 0.336 for figure 3.5(a) and (b) respectively. The peak that can be seen at around 10,000nm is due to big aggregates in the solution.

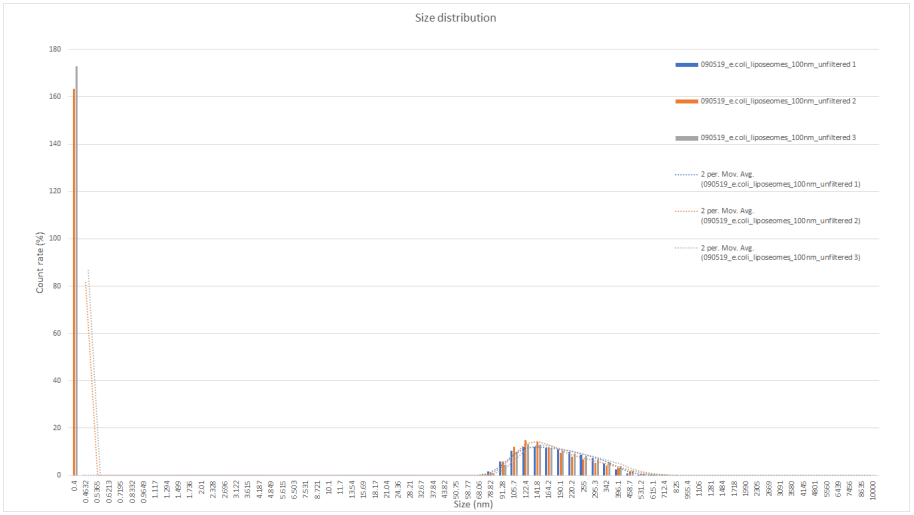

(a)

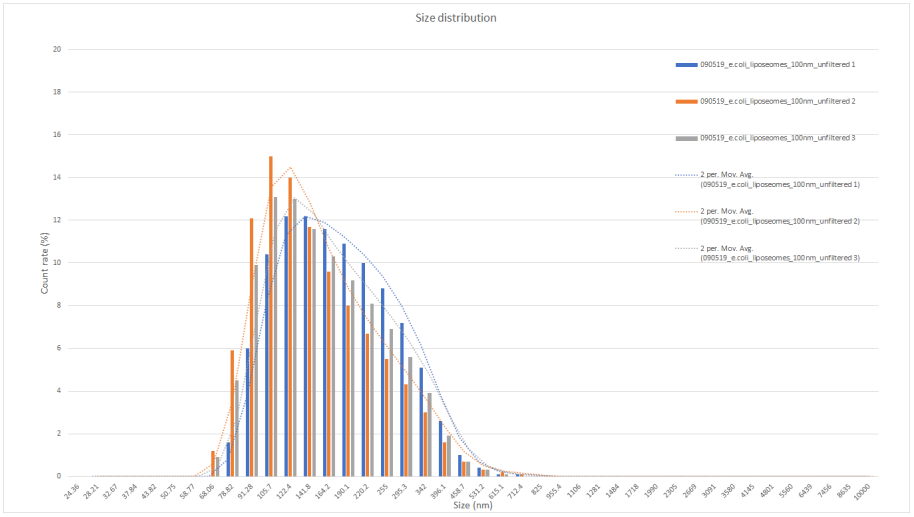

(b)

Figure 3.6: (a-b) These *E.coli* liposomes were made with unfiltered buffer. The measurements gave a polydispersity of 0.46. It can be seen that the sizes of 0.4nm gives the highest intensity (count rate of 160%), indicating that most of the liposomes in the solution is only 0.4nm in diameter or small aggregates of phospholipids are present. Figure (b) have excluded the small fragments of lipids. It can be observed that the average diameter is 122.4nm and only has an intensity of 10%.

It can be observed from figure 3.6, the size which gives the highest count rate in this sample is 0.4nm. The reason for this could be because of small aggregates of phospholipids. If excluded from the graph it can be seen in figure 3.6(b) that the average diameter is 1122.4nm with a count rate of only 10 %.

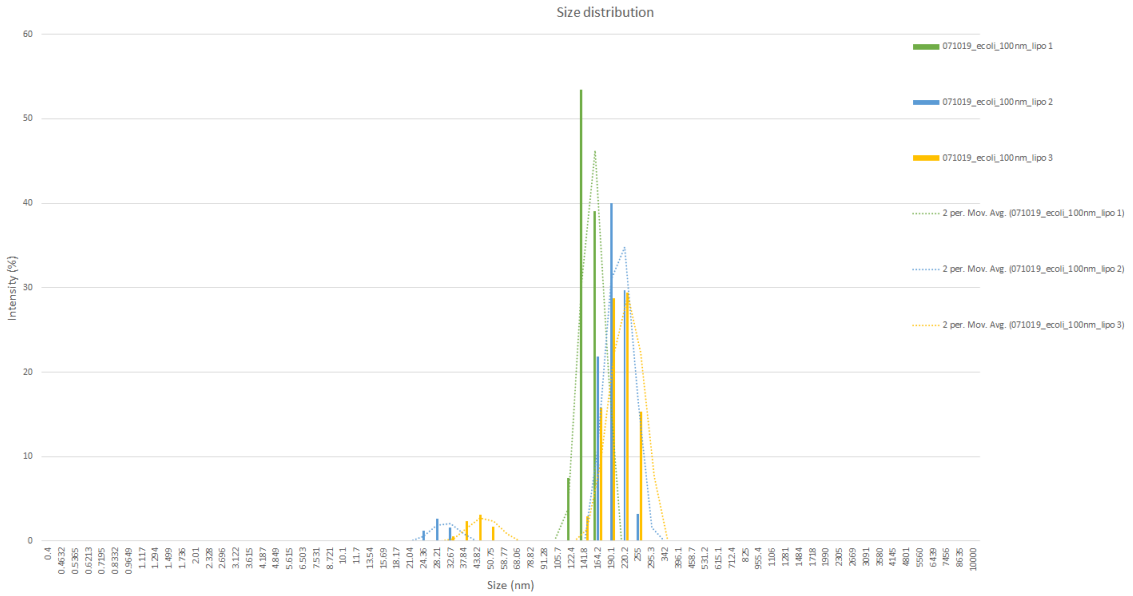

Figure 3.7: *E.coli* measurement with filtered buffer. Small aggregates can be seen but the average size is 164.2nm with a pdi of 0.86

Figure 3.7 is *E.coli* liposomes that have been extruded. Small aggregates are still present and the average size is164.2nm with a pdi of 0.86.

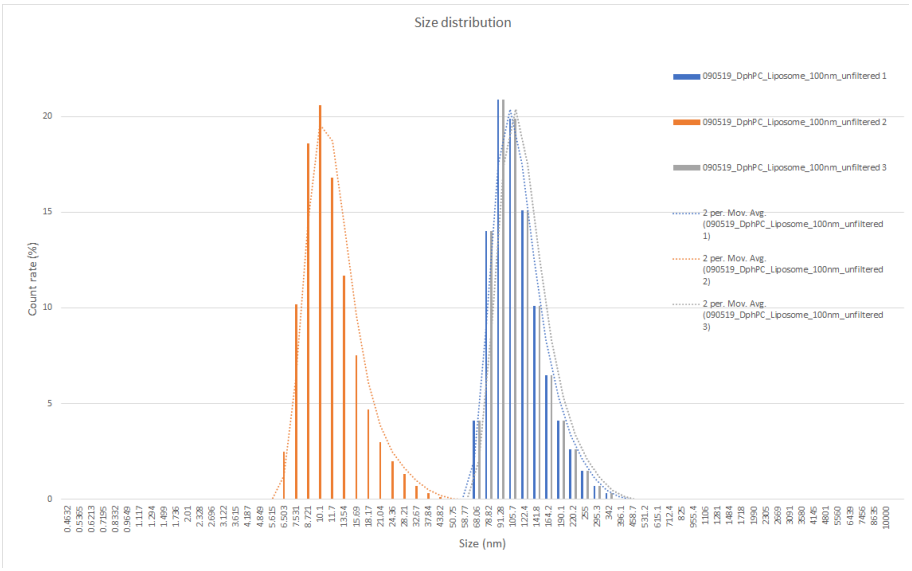

Figure 3.8: DPhPC liposomes were also produced. It can be seen that the average is 91.28 nm if all 3 measurements were averaged. The pdi for the measurement is 0.13

DPhPC liposomes were also produced because the lipids were available in-house. These lipids did give the expected size but were not used further in the study.

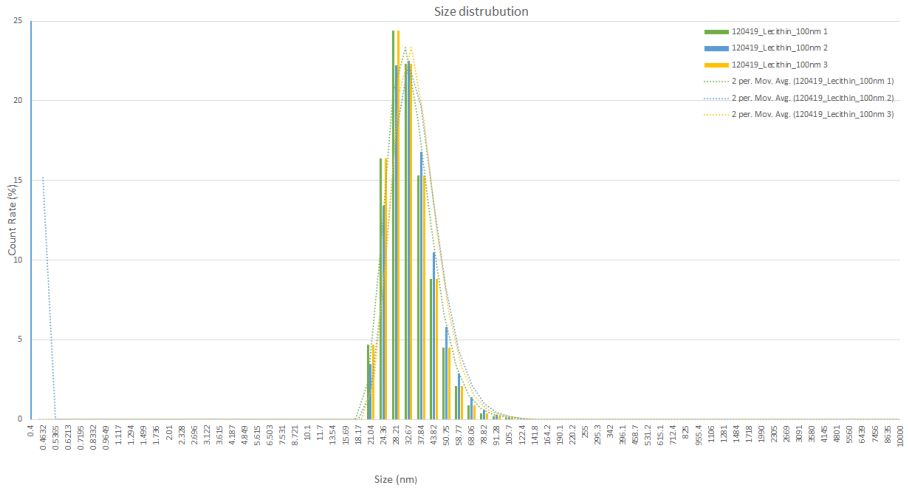

Figure 3.9: It can be observed that small aggregates are still present in ths solution. But the average size is 32.67nm with a pdi of 0.23

Samples from figure 3.5(b), 3.7 and 3.9 were used for further characterization.

3.3 Scanning electron microscope

A scanning electron microscope (SEM) was used to see the morphology of the nanopores. The quality of the surface influences how effective the liposomes can self-assembly into a lipid bilayers.

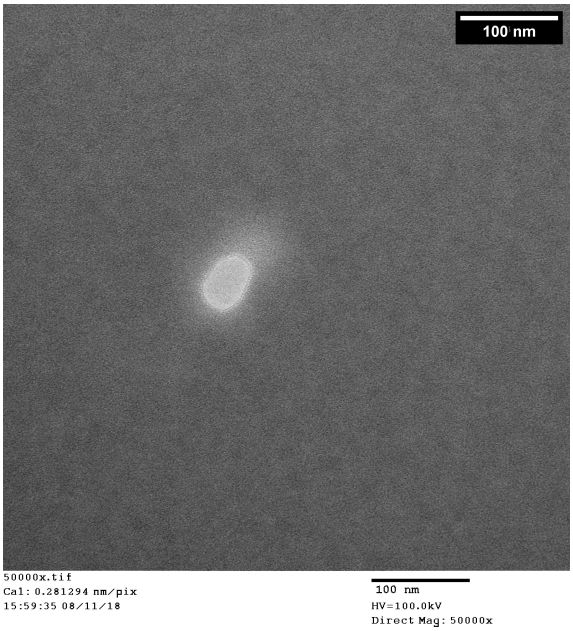

Figure 3.10: A SiN_x nanopore observed under a SEM. Size of the nanopore is 30nm in diameter.

To control the morphology of the nanopore focused ion beam (FIB) was used on undrilled SiN_x substrates. To figure out the correct dose value to make the desired 60nm nanopores,

a 10x10 array was made with an increase of dose value of 2 for every pore.

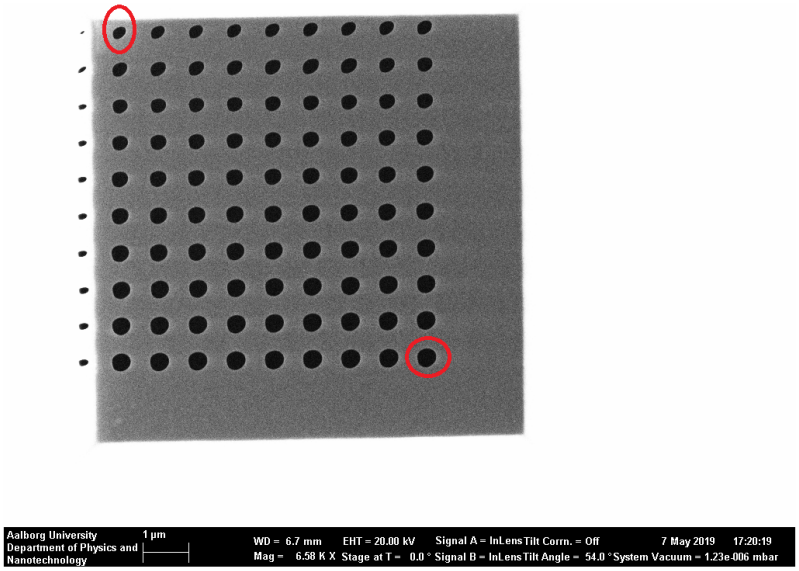

(a)

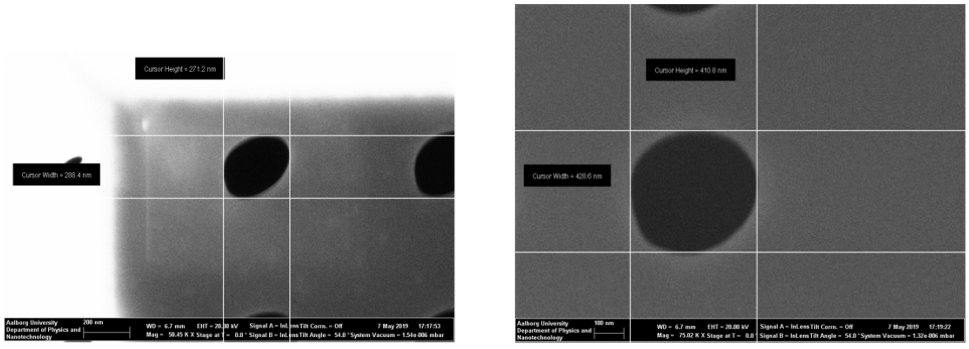

(b) **(c)**

Figure 3.11: 10x10 arrays on a SiN_x substrate. The doses were increased starting from 25 to 233 ions/cm^2 area from the top left corner ending on the bottom right corner. (a) Overview of the array. The red marking are where picture (b) and (c) are focused. (b) Dosis of 27 ions/cm^2 were applied and the height of the pore is 271.2nm and the width of the pore is 288nm. (c) Is the last pore and with the highest dosis of 233 ions/cm^2. The height is shown to be 410.8nm and the width is 428.6nm.

The 10x10 array can be seen in figure 3.11(a) and the red markings represent the nanopores that were looked at in more details (figure 3.11(b) and (c). It can be seen that the first nanopore in the array did not give good morphology but it did get through the substrate.

3.4 Atomic force microscope characterization

3.4.1 Deposition of *E.coli* liposomes Silicon Nitride

A comparison of a clean SiN_x nanopore vs. deposited liposome on the nanopore was performed with AFM. A 5x5μm overview scan of the before nanopore can be seen in 3.12(a) while in figure 3.13(a) is the 5x5μm scan with deposited liposomes. The average

height distribution can be seen in figure 3.12(b) and shows that it is approximately 1.5nm. The height profile for the deposited sample can be seen in figure 3.13(b) and shows that the particle is roughly 13nm height. An average height distribution for after deposition sample is not shown as it yields an average of 0nm.

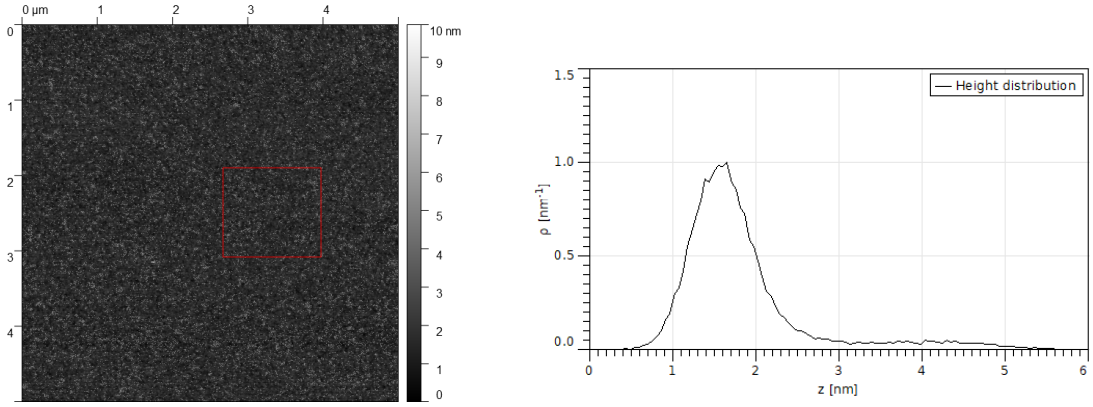

(a) **(b)**

Figure 3.12: (a) 5x5μm overview scan before deposition of a SiN_x nanopore. (b) Height distribution of before deposition.

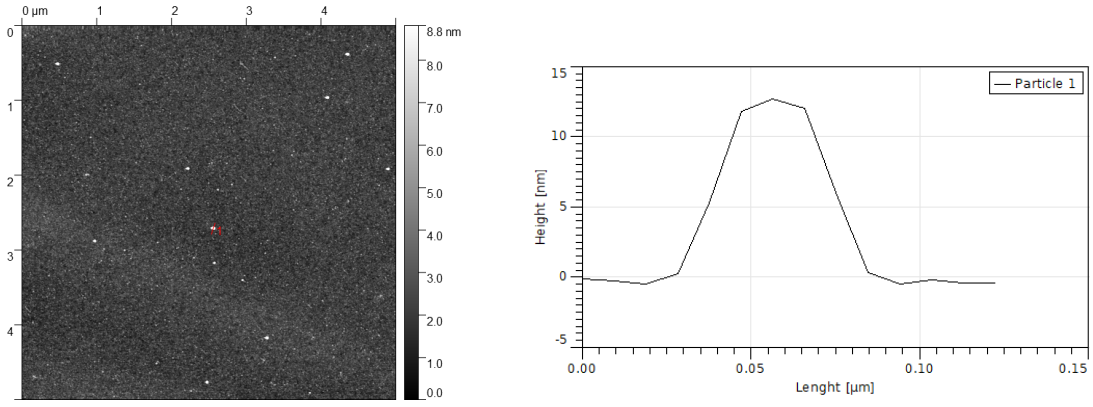

(a) **(b)**

Figure 3.13: (a) 5x5μm overview scan after deposition of a SiN_x nanopore. (b) Height profile of particles in interest.

Reducing the scan to 1x1μm and the small particles can still be observed on the before deposition sample, and the height distribution is unchanged. The 1x1μm scan can be seen in figure 3.14(a) and the height distribution can seen in figure 3.14(b).

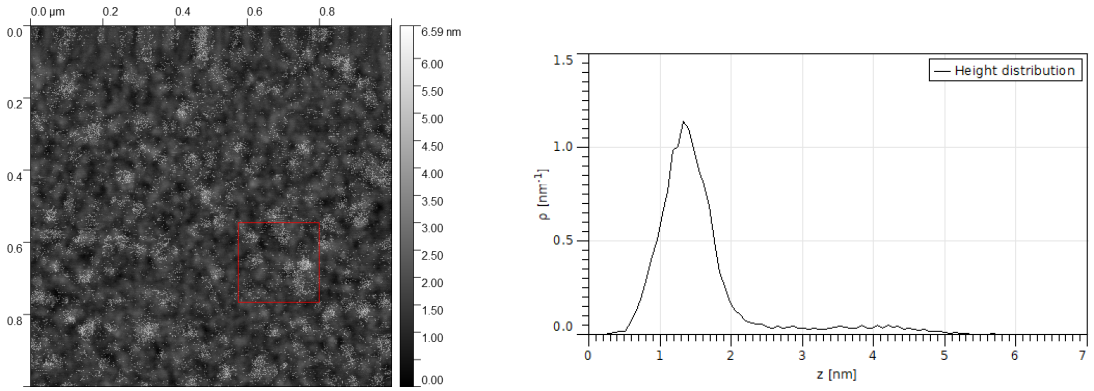

(a) **(b)**

Figure 3.14: (a) 1x1μm before deposition overview scan of a SiN_x nanopore. (b) Height distribution of before deposition.

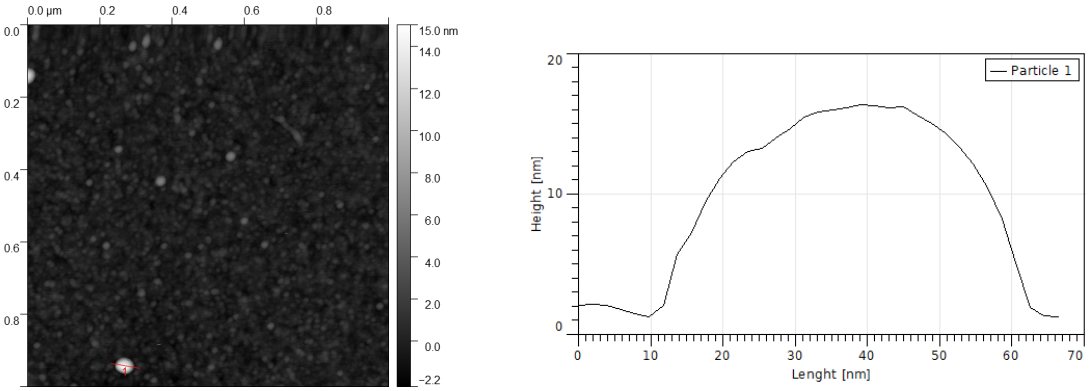

(a) **(b)**

Figure 3.15: (a) 1x1μm overview scan after deposition of a SiN_x nanopore. (b) Height profile of a particle.

Overall the coverage is found to be low on the deposited samples. In both figure 3.13(a) and 3.15(a) no significant increase in coverage is observed. Big particles are observed which suggest the presence of liposomes.

E.coli liposome deposition on modified silicon Nitride

E.coli liposomes were deposited on silicon nitride and characterized. These $SiNx$ substrates were first functionalized with APTMS to make the surface hydrophilic.

The coverage was still good with particles visible. The height profile shows a height of approximately 21nm - 23nm.

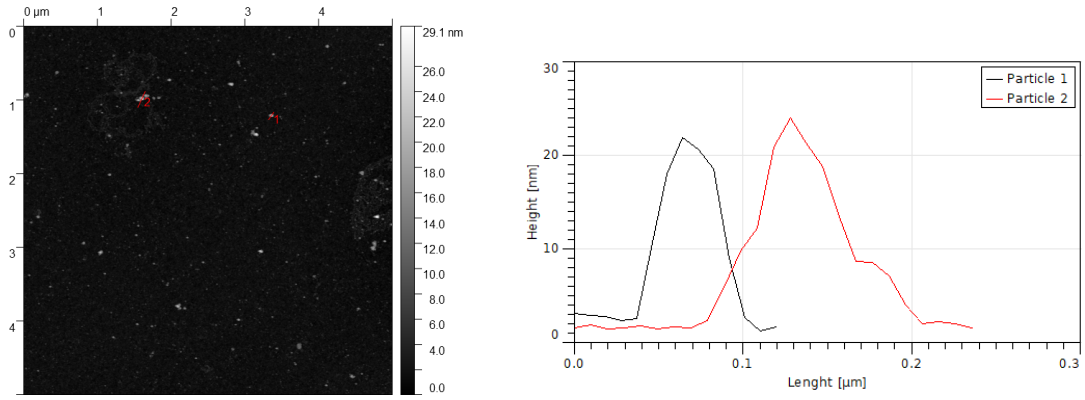

(a) **(b)**

Figure 3.16: (a) 5x5 μm SiN_x substrate overview scan with *E.coli* liposome. (b) Height profile of particles in interest

3.4.2 *E.coli* liposomes deposition on mica slides

Fresh made *E.coli* liposomes were deposited on freshly cleave mica slides seen in figure 3.17(a).

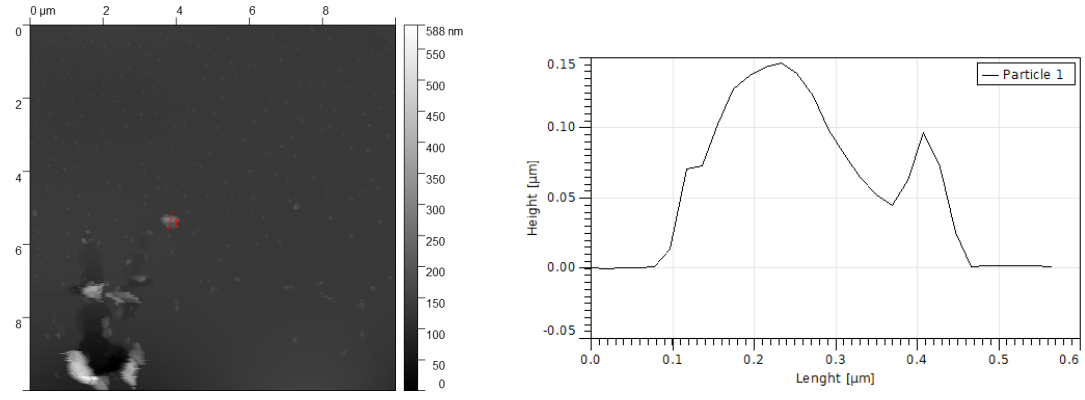

(a) **(b)**

Figure 3.17: (a) 10x10μm overview scan of liposomes on mica slides. (b) Height profile of particles in interest.

As seen in figure 3.17(a) good coverage was obtained and particles can be seen.

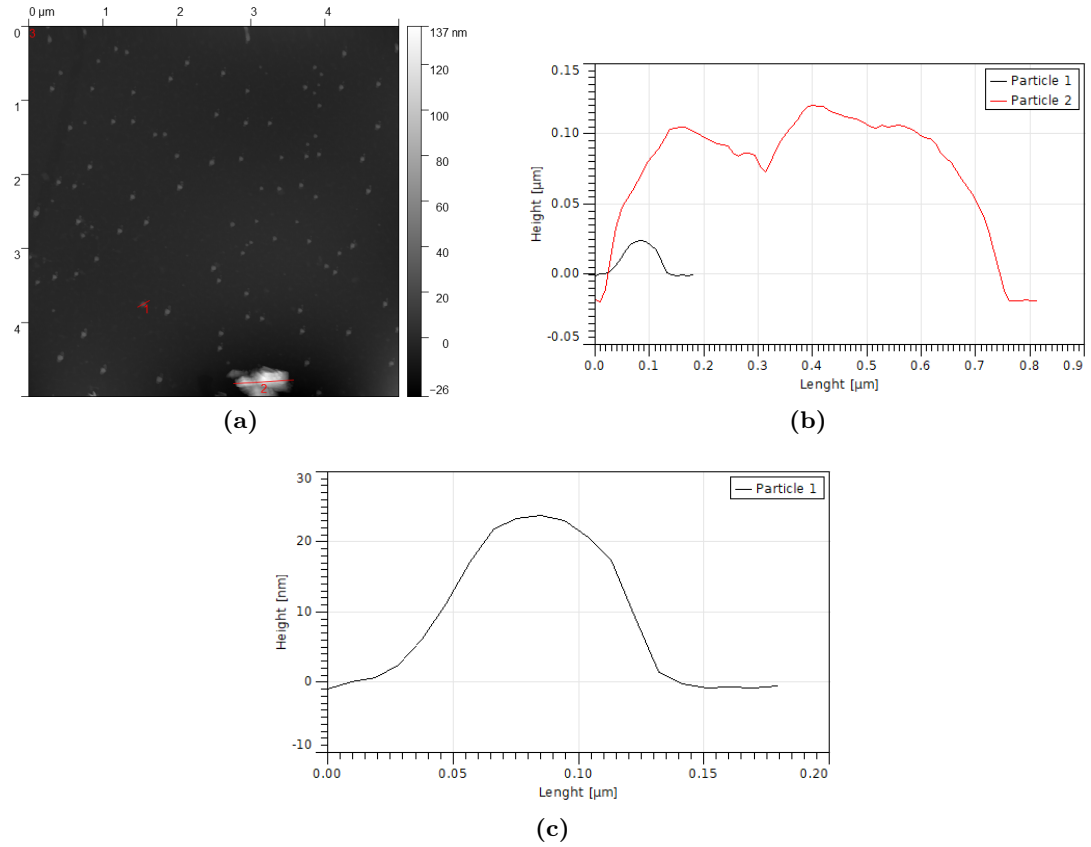

Figure 3.18: (a) 5x5μm overview scan (b) Height profile of particle in interest. (c) Particle 1

A 5x5 scan was then performed, figure 3.18(a), to investigate the height of these particles. In figure 3.18(b) shows these particles are in the range of 21-23nm. Particle 2 in figure 3.18(b) is in the range of 100nm which is either crystal structures from the KCl buffer or aggregates of liposomes.

3.4.3 *E.coli* liposome deposition on a SiN_x 10x10 array

The liposome was deposited on SiN_x substrates where the pores were made in-house. The arrays were made in order to find the optimal dose to drill a nanopore less than 100nm in diameter.

It can be seen in figure 3.19(a) that structures are visible and on the arrays of nanopores but due to the shape it might be contaminant or crystal structure from the KCl buffer. In figure 3.19(b) the height is bigger than 100nm which indicates contaminant and not liposomes.

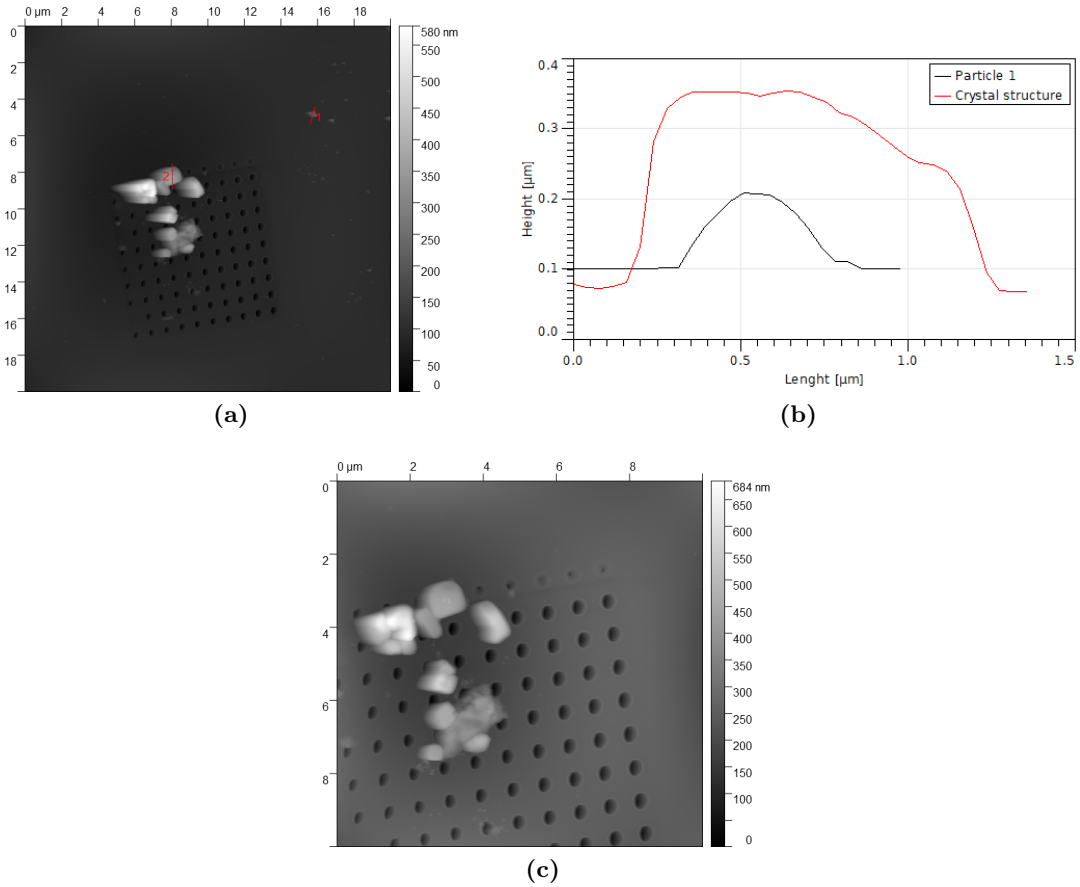

(a) **(b)** **(c)**

Figure 3.19: (a) 20x20μm overview scan of liposome deposition on SiN_x with a 10x10 array structure. (b) Height profile of particles in interest. (c) 10x10μm over scan.

Top left of the corner of the array is the small nanopore with a low dose and the bottom right with the highest doses and biggest nanopore.

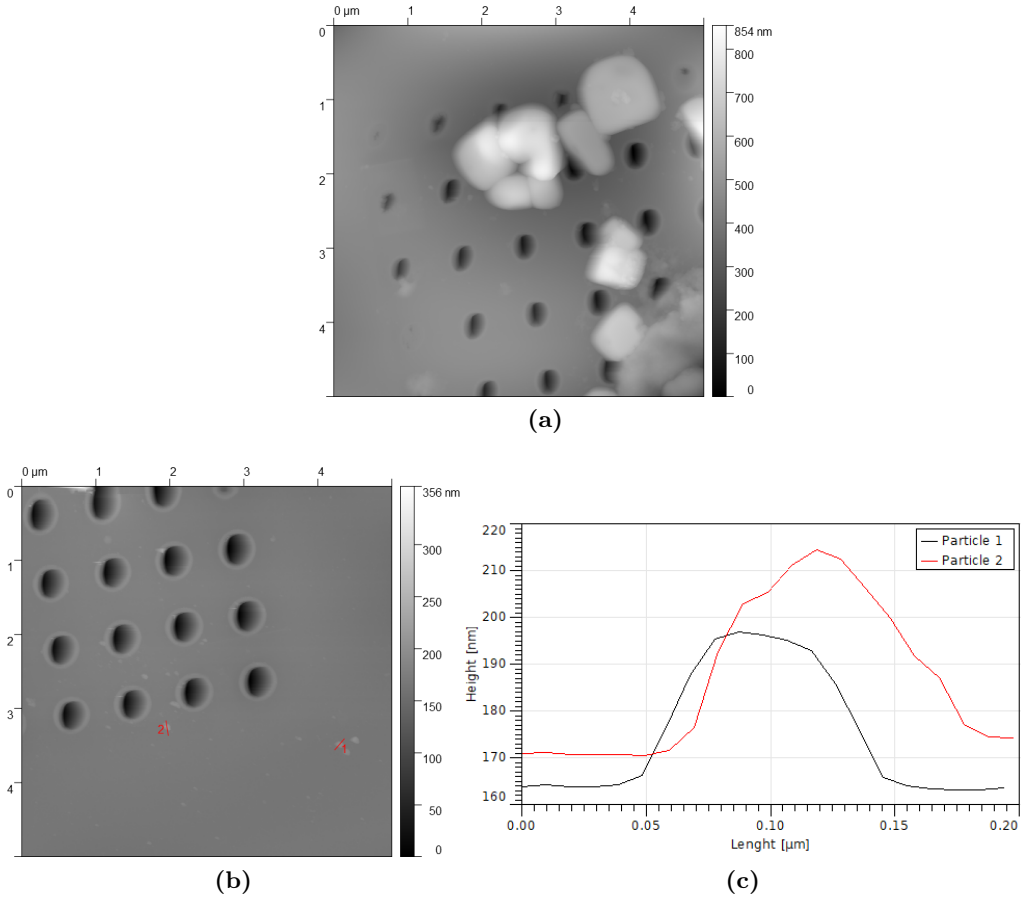

(a) **(b)** **(c)**

Figure 3.20: (a) Bottom right corner. Shows the highest dosis of 233. The width is 428nm amd the height is 410.8nm (b) Bottom right corner of the array after deposition. (c) Height profile of particles in interest

3.4.4 *E.coli* liposome deposition after bilayer formation measurement

Imaging of undrilled SiN_x substrates with AFM was done right after electrochemical measurements to check for leakage.

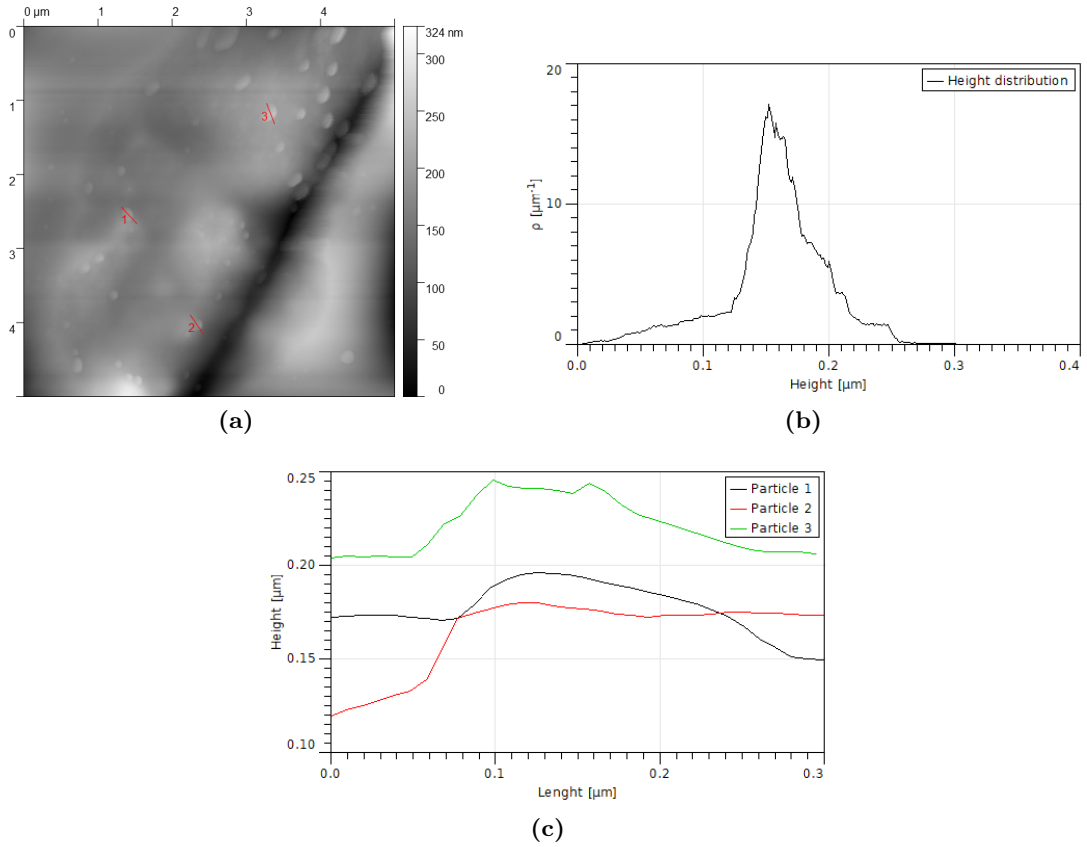

(a) **(b)**

(c)

Figure 3.21: The charaterization of undrilled SiN_x nanopores were done right after bilayer formation measurement in order to check for leakage. (a) 5x5 μm overview scan. (b) Average height distribution. (c) Height profile of particles in interest.

Even though the surface of the substrate is rough, as seen in figure 3.21(a), the presence of a hole on the surface was not observable. The average height can be seen in figure 3.21(b) and is measured to be approximately 150 - 160nm. Relevant particles have also been measured as seen in figure 3.21(c).

3.4.5 Lecithin deposition on silicon oxide

Lecithin were deposited on silicon oxide (SiO_2) substrate and characterized.

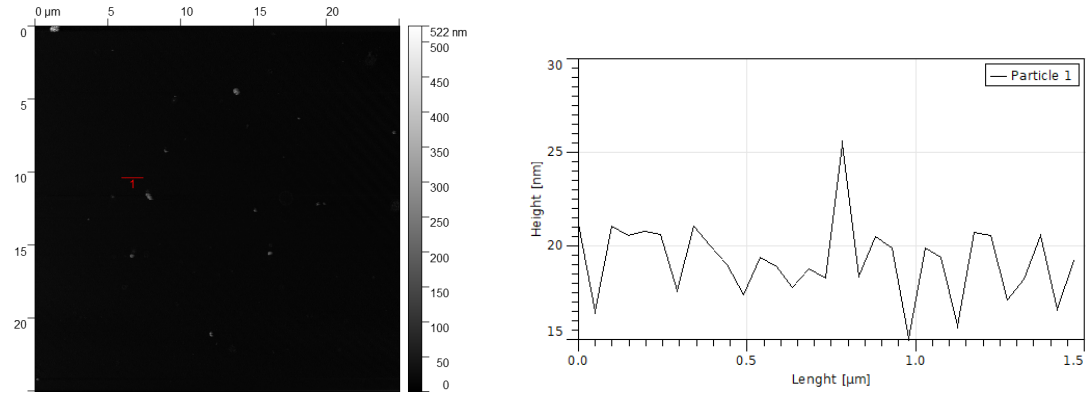

(a) **(b)**

Figure 3.22: A control sample were first measured. Big particles on the surface can be seen but from the profile, smaller particles can be observed. (a) 23x23 μm overview scan. (b) Height profile of particles in interest.

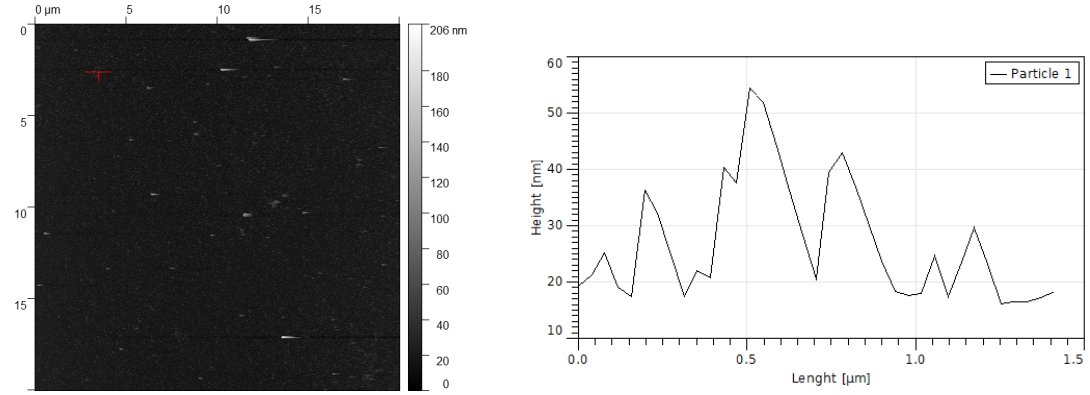

(a) **(b)**

Figure 3.23: Deposition of lecithin on Si_O2. Big particles can be observed on the surface. These particles might be contaminants (a) 20x20 μm overview scan. (b) Height profile of particles in interest.

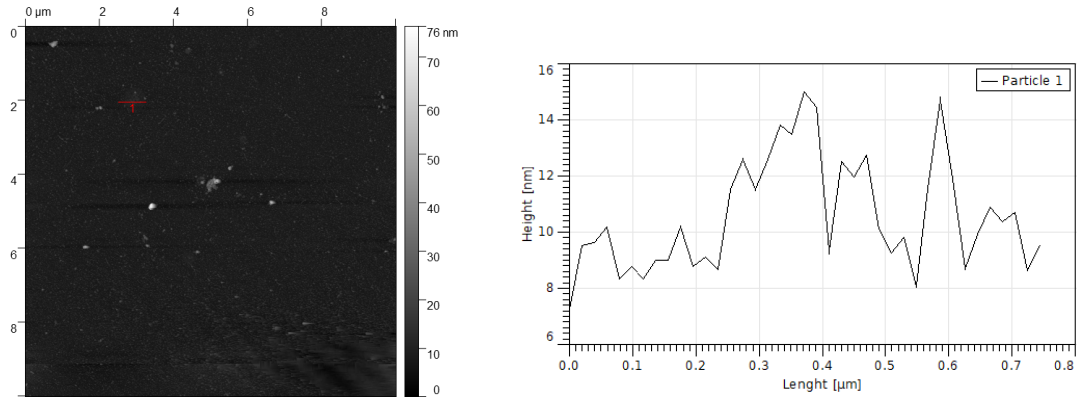

(a) **(b)**

Figure 3.24: Big particles can be observed on the surface as well as small particles suggesting good coverage of lecithin. (a) 10x10 μm overview scan. (b) Height profile of particles in interest.

On figure 3.24(b) it can be seen that the height of some of the particles are on 9 nm in height. This suggest that lecithin liposomes are deposited on the surface with good coverage

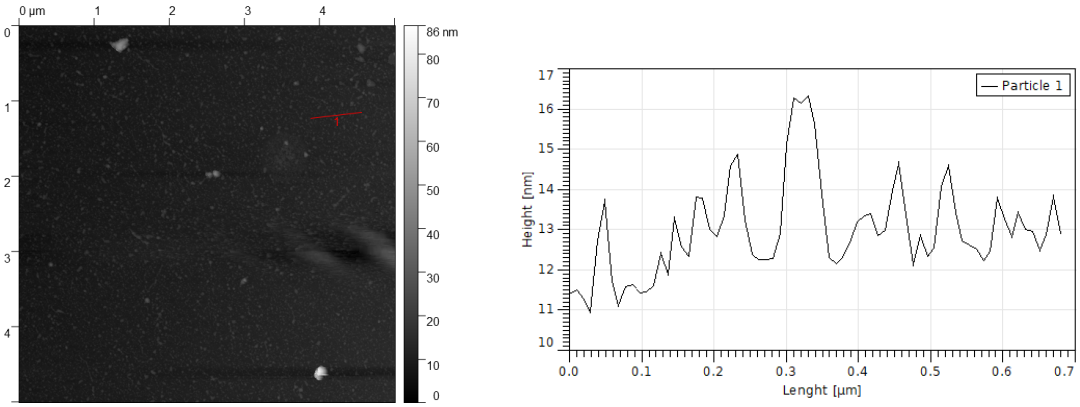

(a) **(b)**

Figure 3.25: The height of the particle has been measured to be 2nm (a) 5x5 μm overview scan. (b) Height profile of particles in interest.

On figure 3.25(b) the profiles show the particle of interest to have a height of 2nm, but with a very flat surface. From the phase measurement (Not shown) a round and flat particle were observed. These structures are likely to be liposomes but due to the shape and flat area, it could be a lipid that is in its gel phase.

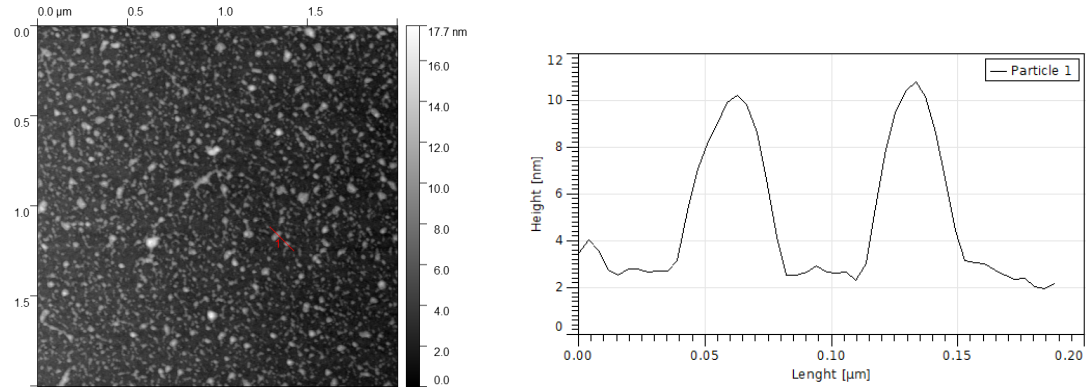

(a) **(b)**

Figure 3.26: 2x2 scan shows good coverage of lecithin vesicle. The height has been shown to be 6nm (a) 2x2 μm overview scan. (b) Height profile of particles in interest.

As seen in figure 3.26 the height of the particle in interest is shown to be 6nm. The height profile shows two particles close to each other and it shows they both have the same height.

3.5 Electrodeposition of silver wires

Electrodepositon of chloride to make Ag/AgCl wires was done. This experiment was performed every time, an electrochemical measurement was planned for the day, as the Ag/AgCl had to be freshly made. Figure 3.27 is shown as the result is the same for each measurement

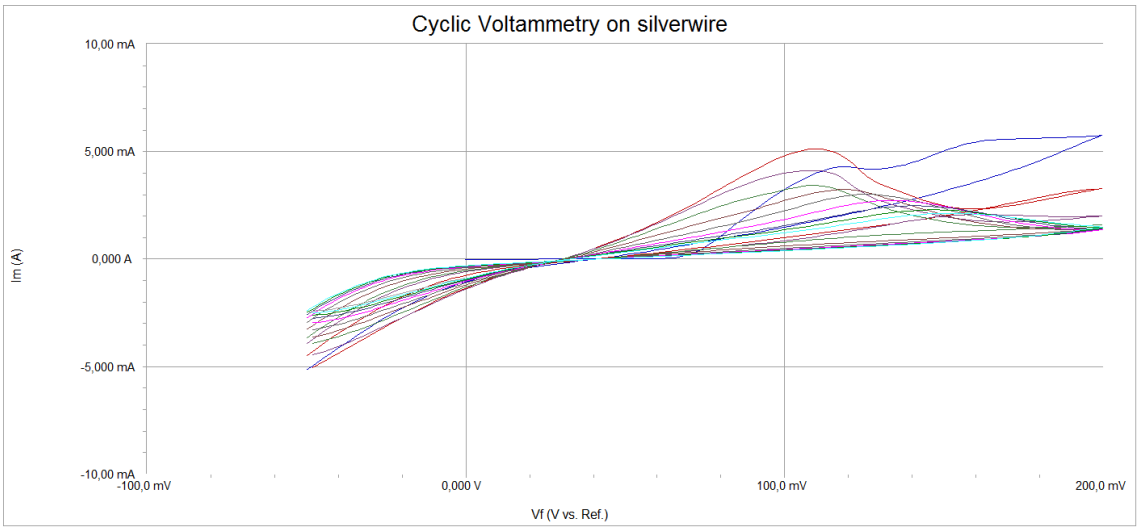

(a)

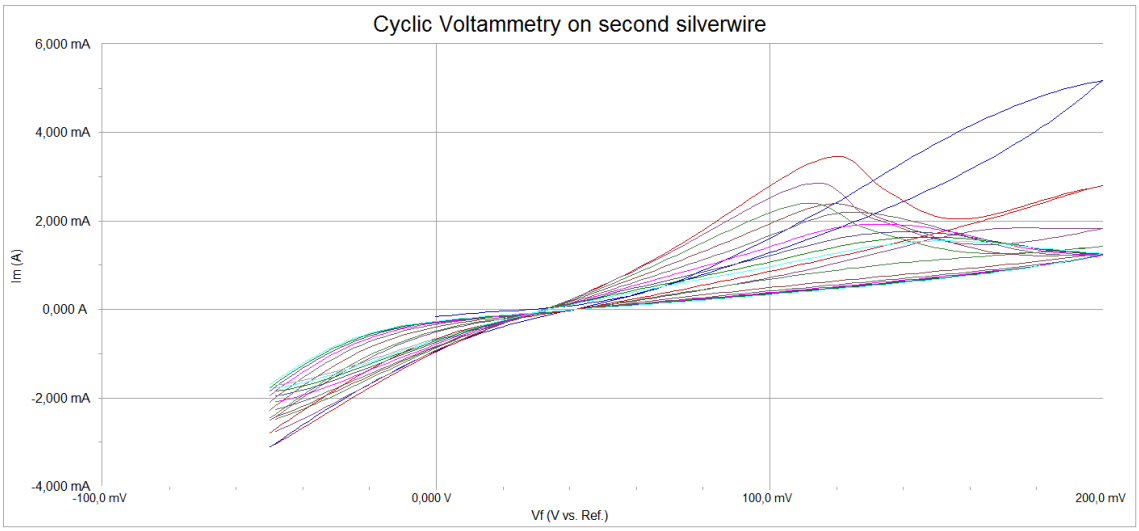

(b)

Figure 3.27: Electroplating of Ag/AgCl wire. The peak is greatest on the forward cyclic making sure that more chloride are deposited on the working electron (Silver wire) making Ag/AgCl. (a) Cyclic voltammetry on wire 1 and (b) cyclic voltammetry on wire 2.

It is observed from figure 3.27(a) and (b) that there is a peak around 100mV which suggest good electroplating of chloride.

3.6 Formation of supported lipid bilayer

The formation of a nanopore-spanning bilayer was done by depositing 60μL *E.coli* liposomes on SiN_x nanopores (unless otherwise stated). All measurement was done with protocol 1 from Elements with functionalized SiN_x surface.

3.6.1 Deposition of *E.coli* liposomes on SiN_x nanopore

The produced *E.coli* liposomes were deposited on a 30x60nm SiN_x nanopore. In figure 3.28 the open square-wave can be observed and no formation of lipid bilayer over time can be seen.

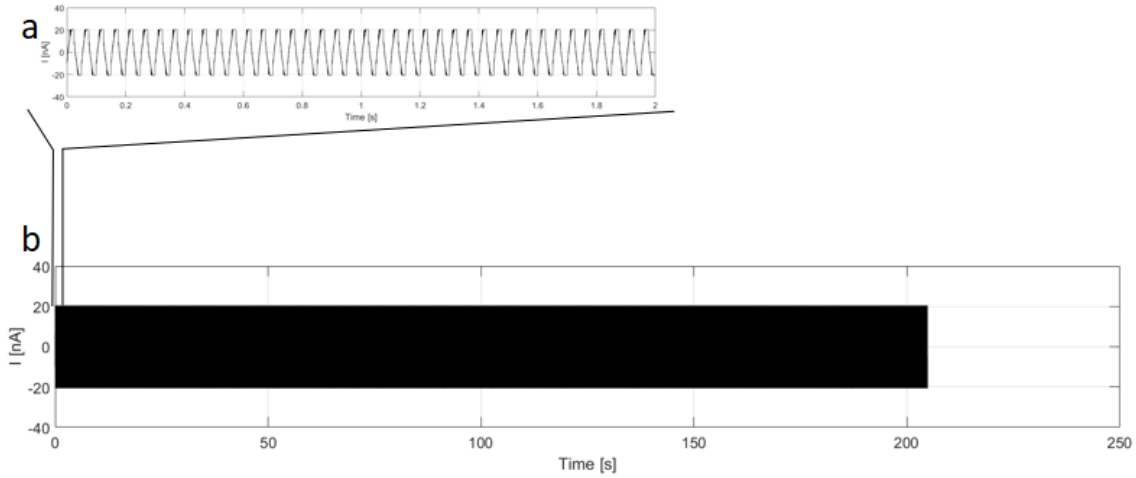

Figure 3.28: Deposition of *E.coli* liposomes on a 60x30nm SiN_x nanopore. No formation of bilayer membranes were observed.

The measurement was redone after rinsing the substrate with water and 70% ethanol and deposited with the same batch of liposomes.

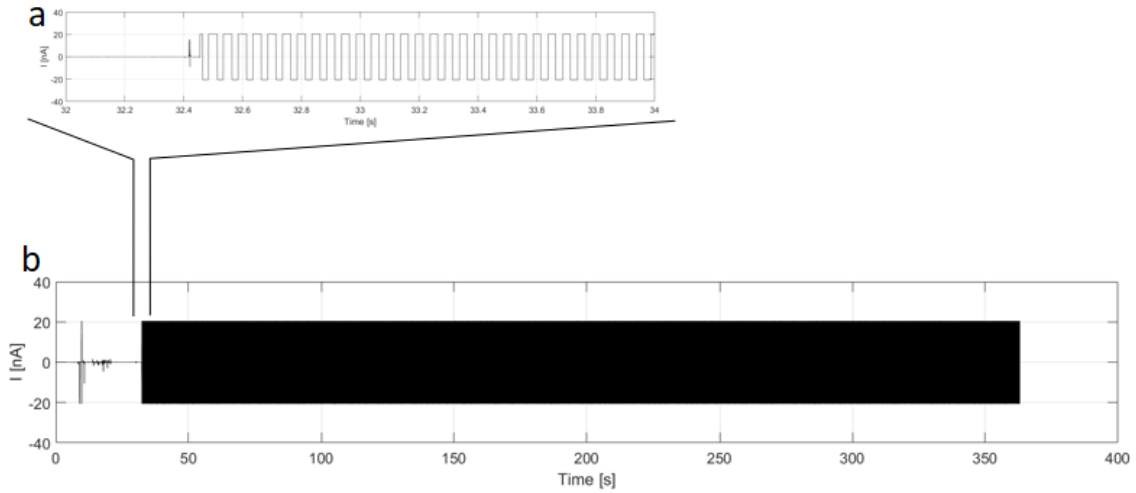

Figure 3.29: New measurement after rinsingThe buffer was added after 8 second, and *E.coli* liposomes were deposited shortly after. No formation was seen.

It can be seen in figure 3.29 that square-waves are present after depositing *E.coli* liposomes. The measurement was started before adding the electrolyte thus no current was observed for 8 seconds and *E.coli* lipid was deposited shortly after. To make sure that the liposomes are covering the nanopore, they were deposited directly on the pore before submerging it in electrolyte and recording as seen in 3.30.

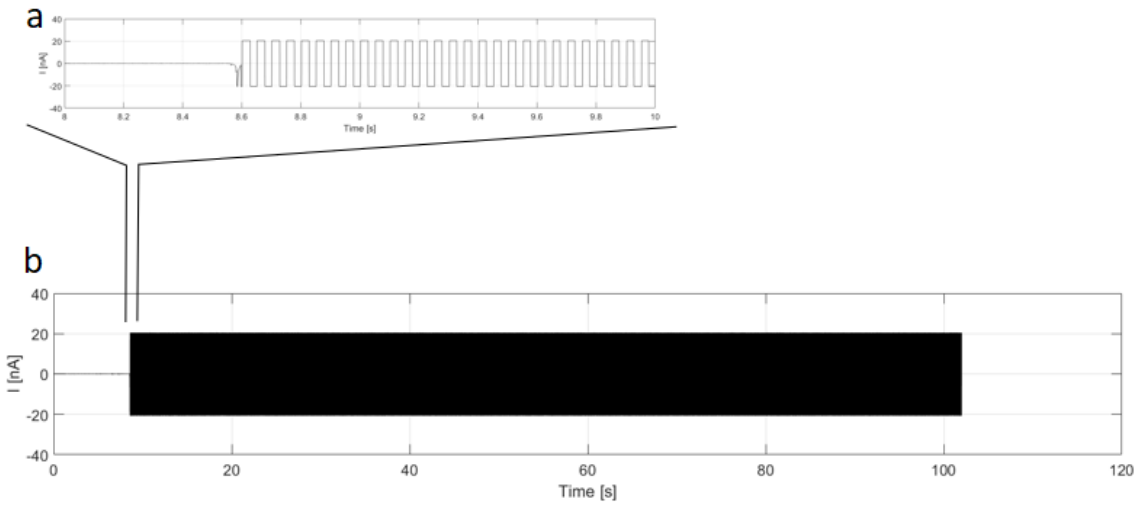

Figure 3.30: Deposition of liposomes were done before the start of the measurement.

The measurement of depositing of liposome directly on the surface of the SiN_x substrate did not yield any difference from previous measurements as can be seen in figure 3.30(a) and (b). be

3.6.2 Free standing *E.coli* lipid membranes

Due to measurements with *E.coli* liposome showed no formation of lipid bilayers by liposome fusion, the painting of lipids dissolved in chloroform/methanol solution was performed, creating free-standing lipid membranes.

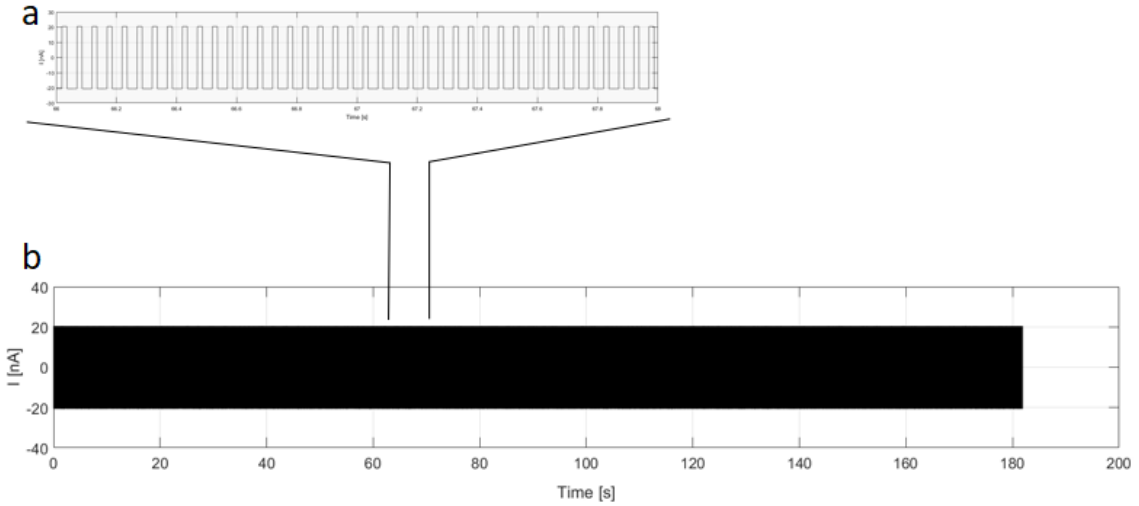

Figure 3.31: Lipids dissolved in chloroform/methanol was painted on the nanopore. A reduction in current did not occur as square-waves are still observable.

As seen in figure 3.31(a) the formation of bilayers did not occur, while figure 3.31(b) shows the square-waves. This meant that the formation of a bilayer formation did not occur as it was expected the current to drop to a triangular wave.

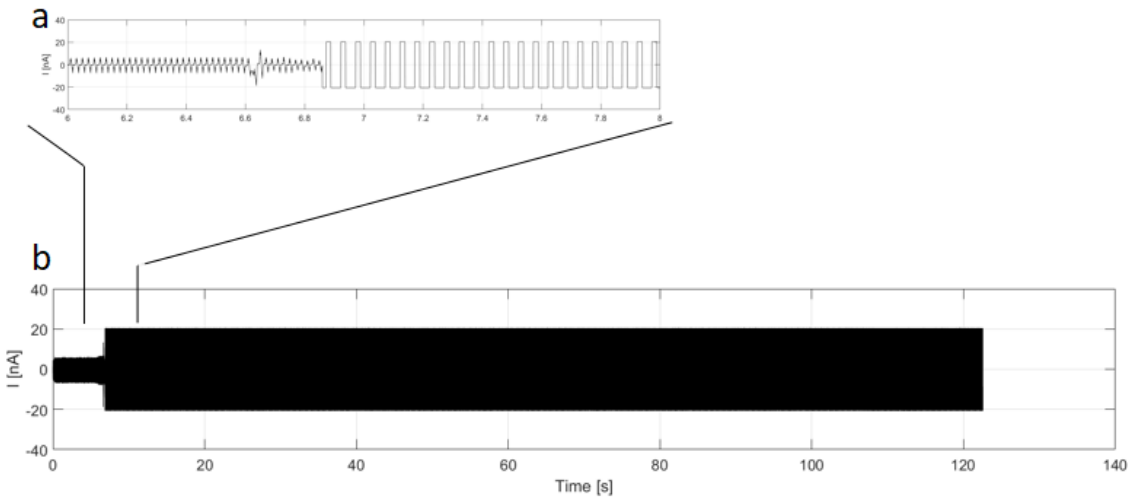

Figure 3.32: *E.coli* liposomes were painted directly on the nanopore before measurements. No formation of bilayers were observed.

Following this result, the liposomes were directly painted on the SiN_x nanopore before the recording of measurement but the formation of lipid bilayers was not observed as seen in figure 3.32(a).

3.6.3 Leakage check measurement

A measurement was performed with an undrilled SiN_x nanopore to see if the current would still be a saturated square-waves or it would be a triangular-wave pattern as there would be no direct contact between the chambers.

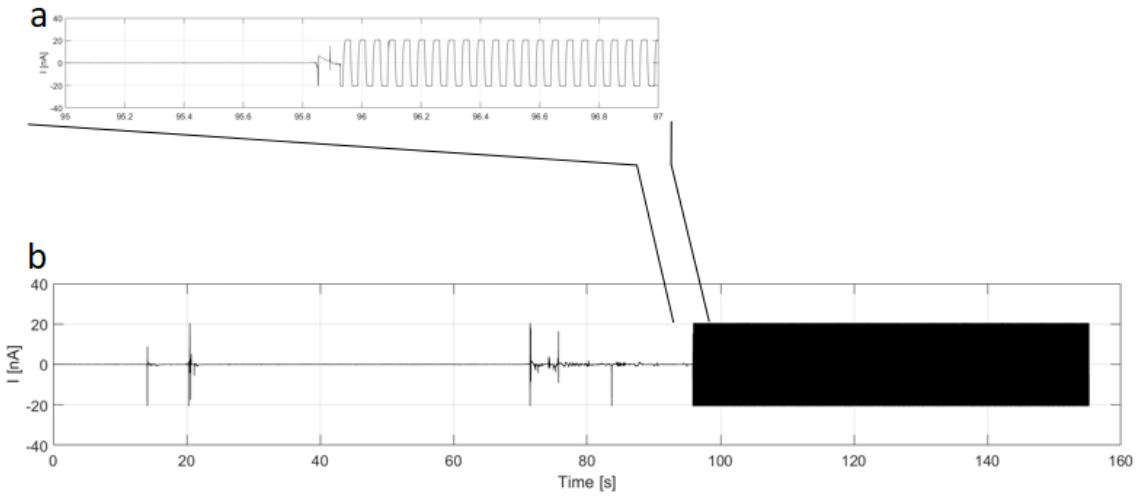

Figure 3.33: Measurements with an undrilled SiN_x nanopore show no change in current.

With the undrilled SiN_x substrate it can be seen in figure 3.33 that the square-waves are still present. This suggests that leakage is present between the two chambers.

Another measurement was performed to double-check the leakage. This was done by physical taping one side of the window of the nanopore cassette with teflon tape as seen in figure 3.34

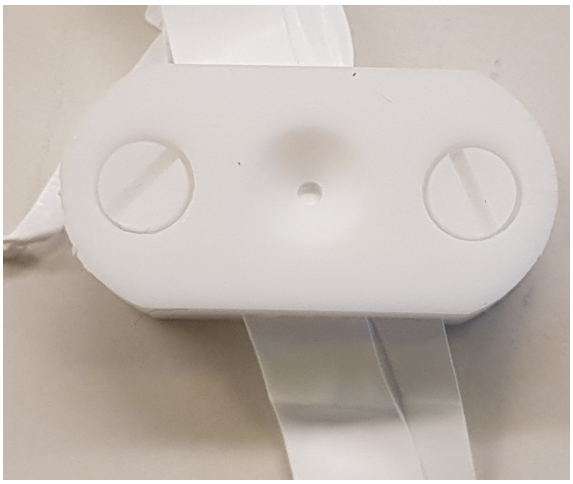

Figure 3.34: Using teflon tape to cover one of the windows on the nanopore cassette, effectively sealing one side of the flow chamber. This makes sure that it is not the screws on the chambers that are the reason for the leak

This resulted in the following measurement

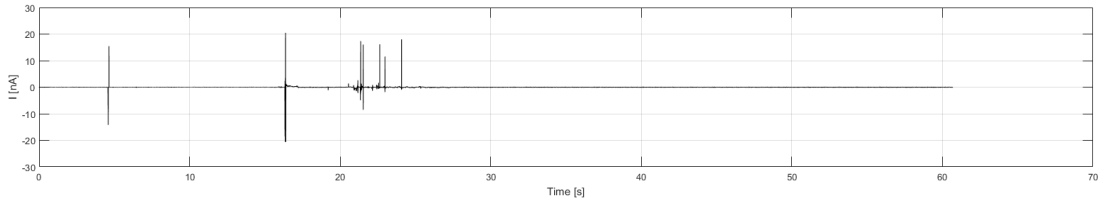

Figure 3.35: The current is not saturated at 20nA anymore, and shows immediately that no connection between the two chambers are connected.

As seen in figure 3.35 no current is saturated and it was decided that new O-rings was needed to prevent leakage.

3.6.4 Depositing lecithin by depositing directly into the window

This method was done because it was closer and easier to gain have access to the surface of the SiN_x. 5 μL lipid solution was deposited directly onto the eye of the cassette before

assembly. It was observed that bubbles were created upon contact with a small amount of water.

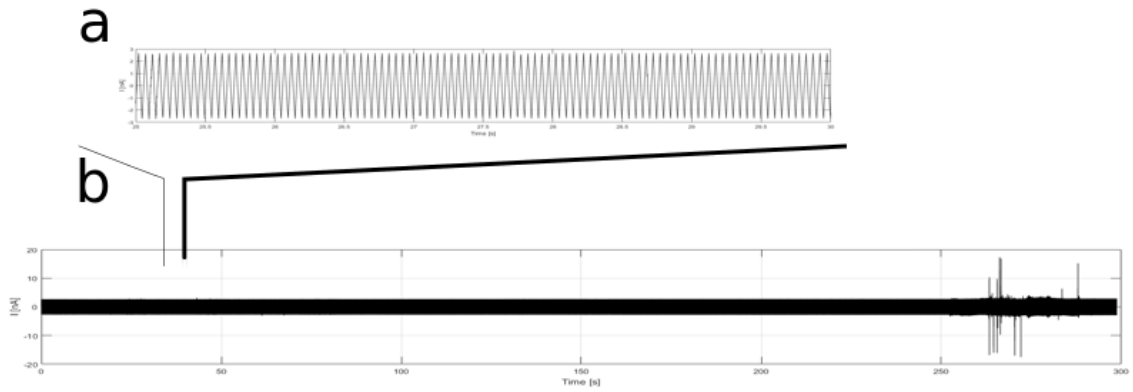

Figure 3.36: The current has dropped but not as significant as when we sealed the cassette. It can also be seen on (a) that the current does not give square-waves as expected when formation of bilayer happens

As seen in figure 3.36(b) the current has dropped and is not saturated at 20nA anymore. Still, this is not the formation of bilayer that is measured but simply an air bubble is partially blocking the signal this reducing the current. On figure 3.36(a) no square wave can be observed as expected when the formation of the lipid bilayer is present.

3.6.5 Deposition of *E.coli* on SiN_x with new O-rings

A new measurement with *E.coli* has been performed with new o-rings.

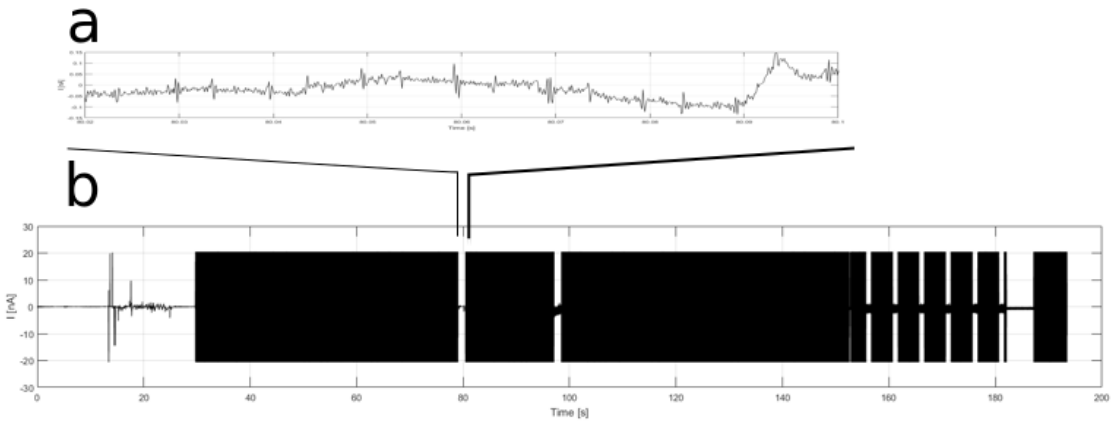

Figure 3.37: It can be seen that the current drops drastically. If zoomed in (b) it is observed that they are not square waves.

As observed on figure 3.37(b) it looked like the formation of a bilayer had occurred but on a closer look (figure 3.37(a) it is observed that it is not square waves. Thus the formation of a bilayer did not occur.

3.6.6 Deposition of lecithin on SiN_x

The deposition of lecithin on SiN_x was measured.

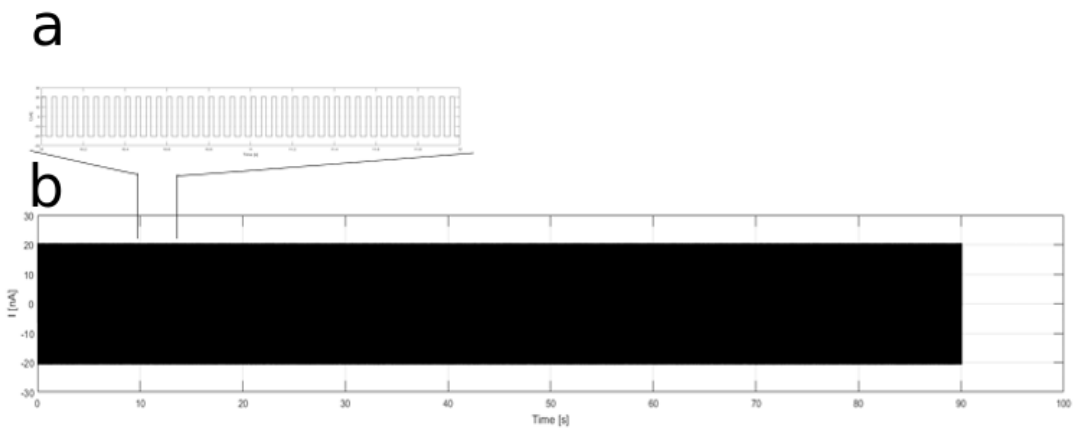

Figure 3.38: No formation of a lipid bilayer occurred even when changed to lecithin. (b) The square-wave saturate at 20nA

As seen in 3.38 no formation of bilayer occurred. The square wave is still present as seen in 3.38(b)

Discussion 4

The ability for *E.coli* liposome to self-assembly into a lipid bilayers on a nanopore and transport ions have been investigated. For the bilayers to transport ions in an electrochemical flow cell, antimicrobial peptides will be used to make a membrane protein. Unfortunately, the self-assembly was not observed and the transport of ions through a bilayer could not be investigated. In the following sections, the results will be discussed. Starting with the characterization of the liposomes, then the surface of the SiN_x nanopores and electrochemical measurements. At the end improvements on the methods will be discussed.

4.1 Characterization of liposomes

4.1.1 Thin-layer chromatography on *E.coli* lipids

To verify the presence of *E.coli* lipids, thin-layer chromatography (TLC) was performed. As mentioned before lecithin was used as a control to verify the presence of lipids. The reason for this is because lecithin is a mixture of different lipids including phospholipids making it a perfect candidate as a control. This also explains why multiple spots can be observed on the silica gel (figure 3.1). The mobile phase used for this measurement was a chloroform/methanol/water solution with the ratio of 65/25/4. According to Avanti polar lipids [47], this ratio is used for general separation of phospholipid headgroup by polarity. The visualization of the spots was done by a destructive method by first spraying the silica gel with a 10% sulphuric acid and then the entire plat was put on a hot plate at 200°C. Brown spots appeared shortly after.

The same mobile-phase were then used to verify the presence of lipids from harvested *E.coli* but no observable spots were seen (3.2(a-c)). This indicates that the mobile-phase dragged the entire sample spot through the silica gel, indicating that the mobile phase was too polar. In figure 3.2(d-e) the ratio was changed to a 75/25/4 and 85/25/10 chloroform/methanol/water solution. Here it was observed that the spot did not move at all. This indicates that the mobile-phase was too apolar and therefore the ratio of the two mobile-phases had to be in between. For the yeast membrane (*Saccharomyces cerevisiae*) (figure 3.3) the same approach with the same mobile phase was used. It was reported by Bui et.al. where they had performed high throughput TLC with the same mobile phase for phospholipid analysis. They managed to get R_f values that were in agreement. They

used a slightly different stain, which was a 10% cupric acid in 8% phosphoric acid, and then burned off at 140°. In this project the use of 10% sulphuric acid has been used. According to [48] in the book "liposomes" the protocol states that 50% sulphoric acid is needed. The reason this staining method is used is because PC and PG lipids will stain brown while cholesterol will have a red-brown colour. As the purpose for doing TLC was check if phospholipid was harvested this method is the most universal. Another universal staining method was to use molybdenum blue spray but that was not available.

The use of a phosphorus nuclear magnetic resonance (pNMR) and mass-spectrometer were also considered but was quickly discarded as it would not produce unusable results since a wide range of different phospholipid are presents in the harvested *E.coli* membrane.

4.1.2 Dynamic light scattering

The preperation of *E.coli* liposomes has been described in section 2.2.6.

To verify the size of the liposomes dynamic light scattering (DLS) was used. The DLS measurements showed sizes below 300nm even though the membrane pore sizes are 200nm. These results show that the unilamellar vesicles should have cycled through the membrane pore during the extrusion process a lot more than 11 times. According to Hope et.al. multiple cycles through the membrane pore will result in mean size of the membrane pore [49]. This is supported further by Ong et.al. [50] where the average size levelled off after multiple cycles. It was also reported that using membrane pore sizes of 200nm of greater the averages size of liposomes would be smaller than the membrane pore size [50]. The biggest limiting factor is the back pressure that the syringes can tolerate, and Hope et.al. reports that to comfortably extrude phospholipids, the concentration has to be less than 20mg/ml and filter pores need to be greater than 200nm [49]. It can be seen in figure 3.5(a) that the average size is shown to be 292nm ± 142.6 indicating that more cycles should have been performed while figure 3.5(b) is shown to be 128nm ± 41.06 and both have been extruded with a membrane pore size of 200nm. A zeta potential was measured for figure 3.5(a) but the zeta potential was found to too low, indicating that they are not stable. It was measured to be -21mV while it should be at least -31mV. Chibowssi and Szczes [51] have shwown that for synthesised lipid vesicle the zeta potential is -56mV

For the lecithin samples the zeta potential was found to be -25mV but due to low concentration of vesicle in the solution no chart was made.

4.1.3 Characterization with atomic force microscope

Before electrochemical measurements the *E.coli* liposomes were imaged in an atomic force microscope (AFM). To distinguish contaminant from dust particle a before and after deposition of the liposomes was performed. It can be seen on figure 3.12 that the average height is 1nm high, are presents compared to to the bigger particles visible (11-13nm

high) on figure 3.13(a). This indicates that the small particles are contaminants while the liposomes would be larger particles. Low coverage was observed on the substrate because, when removing the excess buffer after deposition, the rinsing could have dragged most of the liposomes of the substrate. Small contaminants are cleaned before during electrochemical measurements due to the rinsing procedure with piranha solutions. This leads to another problem due to the fact that the organic silane structures get destroyed during the process as well.

Deposition of liposomes on mica slides

The liposomes were also deposited on mica slides to see the coverage and morphology of the liposomes (figure 3.18(a)). Better coverage can be observed but no total coverage was achieved. In figure 3.18(c) the height of the liposome is 20nm and the diameter is 50-110nm which is what is expected from liposomes with sizes of 25-125nm according to Richter et.al. [52]. This particle can also be multiple vesicle stacked op top of each, when the liposomes are in the gel-phase. According to the company Avantii [53] the glycerophospholipids have different phase transition temperature. As the vesicle is build up from different phospholipid structures, it is unsure if it in the gel-phase or not. Richter et.al. also reported that at low coverage a low probability of formation of lipid bilayer would occur. Only subsequently scans after shows the correct the expected sizes of the liposomes. Due to the low coverage of the liposomes the formation of supported lipid bilayers by fusion of liposomes were not observed [52]. Picas et.al. [26] have reported that height for a vesicle in gel-phase is only 4 nm heigh. Richter et.al. reports that vesicles with high negative charge would form a vesicle supported bilayer at high concentrations due to the electrostatic force between the neighbouring vesicles making the following deposition harder.

Deposition of liposomes on SiN_x substrates

Deposition of *E.coli* on SiN_x substrates were also performed. The same particle sizes can be seen, with roughly 20nm in height and a diameter of approximately 80nm can be seen (figure 3.16(b)). Generally, the same structures can be found on the SiN_x substrates indicating that bilayers are present.

In order to check for leakage an undrilled SiN_x substrate were measured right after electrochemical experiments 3.21(a). A lot of particles can be observed and most of them are in the range of 100nm in height. These particles are most likely crystal structures from the electrolyte used during experiments. It can be observed that the surface of the nanopore is rough, which is not favourable for supported lipid bilayer formations [3]. Imaging this substrate was difficult but no holes on the substrate were observed indicating that a leak during the electrochemical experiments was likely.

During the imaging of SiN_x substrate with a 10x10 array, no proper deposition could be

observed. Due to the crystalline structures seen figure 3.20(a) it is assumed to be from the buffer. Though some of the nanopores seem to have been covered. According to Korman et.al. the formation of nanopore-spanning bilayers requires a vesicle diameter larger than the pore diameter [3]. Due to the wide range of liposomes sizes, some of the nanopores are plugged, though this does not exclude the probability of the pore being blocked by the buffer as only the first couple of row are blocked or partially blocked. With the bigger diameter, no blockage was observed during the imaging with AFM as seen in figure 3.20(a). This presence of crystalline structures can also be verified on figure 3.20(b) as the height of the particles are shown to be over 150nm.

4.2 Formation of supported lipid bilayers

The formation of a nanopore-spanning lipid bilayer with *E.coli* liposomes were not observed in any of the experiments. The pore diameter is given to be 60nm while it was shown that the liposomes used were larger than the diameter which is a parameter for the formation of lipid bilayer [3]. It is believed that the formation of liposomes bilayer still happened on the nanopore as the general approach has been conducted [3, 54, 55], but formation could not be recorded due to a leakage in the cassette. This leakage was confirmed with the measurements of an undrilled SiN_x (figure 3.33), substrate which gave the same square-wave pattern as with the drilled SiN_x substrates. When imaged with an AFM no holes were shown on the substrate, and the only way a contact could happen between the two electrochemical cells would be if the electrolyte was leaking through. The cassette is fastened by two bolts and if one were to tighten the bolts too much, it would damage the threads and perhaps the bolts were not tightened enough during the experiments.

Another approach to get the formation of lipid bilayer was to deposit lipid solution directly into the window of the cassette. This minimized the distance the lipid had to be attracted to the hydrophilic surface, but air bubbles were observed when the solution was deposited. As seen in figure 3.36 the current has dropped, but on figure 3.36(b) non-square wave are observed. Another measurement was performed where one side of the window to the cassette was sealed off with teflon tape (3.35. This confirmed the suspicion of damaged o-rings. The damage o-rings might be due to wear and tear, but also during cleaning with piranha solution. The problem could have been the surface around the nanopore is too rough, making it hard for the lipid to attach and form a bilayer [56].

4.2.1 Improvements of experiments

To get better coverage, the use of AFM measurements in liquid could have been used as Richter et.al. reported [52]. This eliminates the rinsing of the sample, and better coverage could have been observed. The use of an AFM equipped with a J-scanner would be necessary to measure the deposition in water. Another method to verify the formation of supported lipid is the use of ellipsometry, quartz crystal microbalance with dissipation

[52, 57], as well as incorporating a fluorescence labelled lipid [3]. During this project the incorporation of an ion pore channel from a pore-forming antimicrobial (AMP) to study the transfer of ions, but other methods could have been used. Instead of fusing liposomes to a surface or making free-standing lipids and afterwards incorporate the AMP, the use of a proteoliposome could have been employed [58]. Demarche et.al. also reported that the electrochemical measurements were also possible by using a whole-cell patch-clamp [58]. A different preparation of supported lipid bilayer could have been used. As reported by Picas et.al. and Rinia et.al. [26, 32] the use of L-B/L-S to make the bilayer could have been a straight forward method. This method also works for porous substrate, and with L-B/L-S method the need to modify substrate surfaces would not be required. This reduces the time needed and one can install the substrate directly onto the cassette. The use of tethered supported lipid bilayer did not work in this project since cleaning the surface of the substrate required the use of piranha solution.

Conclusion 5

In this project, the investigation of nanopore-spanning lipid bilayers with the use of phospholipid liposomes, from *E.coli* and eggyolk lecithin. Unfortunately, the lipid bilayer could not be investigated because the formation of the lipid bilayer was not observed.

In the first part of the project, the extraction of total lipids from microorganisms, mostly *E.coli*, has been performed. To verify the presence of harvested lipids, thin-layer chromatography (TLC) has been performed with different ratios of eluent. *E.coli* liposomes were made by extruding with a membrane pore size of 200nm. The size of the liposomes was measured with dynamic light scattering (DLS) and show sizes of 164nm, 128nm, 122.6nm, and 32.67nm.

The liposomes were characterized in atomic force microscopy (AFM) to see the morphology and coverage on SiN_x substrates. It has been shown, that coverage is low but fusion of liposomes to the surface did occur.

Formation of a lipid bilayer was not observed as the electrochemical measurement showed always showed an open square-wave pattern. This was further tested upon by separating the electrochemical cell with an undrilled SiN_x substrate. The measurements still showed an open-square wave, and the substrate was imaged with AFM for further investigations. New o-rings was installed, but showed no effect.

Bibliography

1. Salehi-Reyhani, A., Ces, O. & Elani, Y. Artificial cell mimics as simplified models for the study of cell biology. eng. *Experimental biology and medicine (Maywood, N.J.)* **242,** 1309–1317 (July 2017).
2. Le, N. T. T. *et al.* Soy Lecithin-Derived Liposomal Delivery Systems: Surface Modification and Current Applications. eng. *International journal of molecular sciences* **20,** 4706 (Sept. 2019).
3. Korman, C. E., Megens, M., Ajo-Franklin, C. M. & Horsley, D. A. Nanopore-Spanning Lipid Bilayers on Silicon Nitride Membranes That Seal and Selectively Transport Ions. *Langmuir* **29,** 4421–4425 (Apr. 2013).
4. MUELLER, P., RUDIN, D. O., TI TIEN, H. & WESCOTT, W. C. Reconstitution of Cell Membrane Structure in vitro and its Transformation into an Excitable System. *Nature* **194,** 979 (June 1962).
5. Glukhov, E., Stark, M., Burrows, L. L. & Deber, C. M. Basis for selectivity of cationic antimicrobial peptides for bacterial versus mammalian membranes. *The Journal of biological chemistry* **280,** 33960–7 (Oct. 2005).
6. Wang, G. *et al.* Antimicrobial Peptides in 2014. *Pharmaceuticals* **8** (ed Vanden Eynde, J. J.) 123–150 (Mar. 2015).
7. Quinn, P. J. A lipid-phase separation model of low-temperature damage to biological membranes. *Cryobiology* **22,** 128–146 (1985).
8. Lubert, B. J. M., L., T. J. & Stryer. *Biochemistry* 7th ed. (ed Jr., G. G. J.) 1054 (W. H. Freeman and Company, 2012).
9. Jackowski, S., Cronan, J. E. & Rock, C. O. in *New Comprehensive Biochemistry* (eds Vance, D. E. & Vance, J. E. B. T. .-.-. N. C. B.) 43–85 (Elsevier, 1991). `http://www.sciencedirect.com/science/article/pii/S0167730608603300`.
10. Van der Rest, M. E. *et al.* The plasma membrane of Saccharomyces cerevisiae: structure, function, and biogenesis. *Microbiological Reviews* **59,** 304 LP –322 (June 1995).
11. Shadiac, N., Nagarajan, Y., Waters, S. & Hrmova, M. Close allies in membrane protein research: Cell-free synthesis and nanotechnology. *Molecular membrane biology* **30** (Jan. 2013).
12. Ott, M., Zhivotovsky, B. & Orrenius, S. Role of cardiolipin in cytochrome c release from mitochondria. *Cell Death & Differentiation* **14,** 1243–1247 (2007).

13. Brown, L., Wolf, J. M., Prados-Rosales, R. & Casadevall, A. Through the wall: extracellular vesicles in Gram-positive bacteria, mycobacteria and fungi. *Nature Reviews Microbiology* **13,** 620 (Sept. 2015).

14. Marquina, D., Santos, A. & Peinado, J. *Biology of killer yeasts* 65–71 (July 2002).

15. Muthuprasanna, P. *et al. Basics and Potential Applications of Surfactants - A Review* (Oct. 2009).

16. Antonietti, M. & Förster, S. Vesicles and Liposomes: A Self-Assembly Principle Beyond Lipids. *Advanced Materials* **15,** 1323–1333 (Aug. 2003).

17. Baeurle, S. A. & Kroener, J. Modeling Effective Interactions of Micellar Aggregates of Ionic Surfactants with the Gauss-Core Potential. *Journal of Mathematical Chemistry* **36,** 409–421 (2004).

18. McGiffen Jr, M., Shrestha, A. & Fennimore, S. in, 89–133 (Jan. 2014).

19. Janiak, M. J., Small, D. M. & Shipley, G. G. Temperature and compositional dependence of the structure of hydrated dimyristoyl lecithin. eng. *The Journal of biological chemistry* **254,** 6068–6078 (July 1979).

20. Stuart, M. & Boekema, E. *Two distinct mechanisms of vesicle-to-micelle and micelle-to-vesicle transition are mediated by the packing parameter of phospholipid–detergent systems* 2681–2689 (Dec. 2007).

21. Zhao, Y. *et al.* Asymmetrical Polymer Vesicles for Drug delivery and Other Applications. eng. *Frontiers in pharmacology* **8,** 374 (June 2017).

22. Tiwari, G. *et al.* Drug delivery systems: An updated review. eng. *International journal of pharmaceutical investigation* **2,** 2–11 (Jan. 2012).

23. Owen, S. C., Chan, D. P. Y. & Shoichet, M. S. Polymeric micelle stability. *Nano Today* **7,** 53–65 (2012).

24. He, H. *et al.* Adapting liposomes for oral drug delivery. eng. *Acta pharmaceutica Sinica. B* **9,** 36–48 (Jan. 2019).

25. Goyal, P. & Aswal, V. *Micellar structure and inter-micelle interactions in micellar solutions: Results of small angle neutron scattering studies* (Apr. 2001).

26. Picas, L., Milhiet, P.-E. & Hernández-Borrell, J. Atomic force microscopy: A versatile tool to probe the physical and chemical properties of supported membranes at the nanoscale. *Chemistry and Physics of Lipids* **165,** 845–860 (2012).

27. Winterhalter, M. Black lipid membranes. *Current Opinion in Colloid & Interface Science* **5,** 250–255 (2000).

28. Bello, J., Kim, Y.-R., Kim, S. M., Jeon, T.-J. & Shim, J. Lipid bilayer membrane technologies: A review on single-molecule studies of DNA sequencing by using membrane nanopores. *Microchimica Acta* **184,** 1883–1897 (2017).

29. White, S. H. Formation of "solvent-free" black lipid bilayer membranes from glyceryl monooleate dispersed in squalene. *Biophysical Journal* **23,** 337–347 (1978).

30. Studer, A. O. *Investigations on planar lipid bilayers in nano-pores to study the function of membrane proteins* Doctoral Thesis (ETH Zürich, 2009), 102. `https://doi.org/10.3929/ethz-a-005901902`.

31. Andersson, J. & Köper, I. Tethered and Polymer Supported Bilayer Lipid Membranes: Structure and Function. *Membranes* **6** (ed Schuster, B.) 30 (June 2016).

32. Rinia, H. A., Demel, R. A., van der Eerden, J. P. J. M. & de Kruijff, B. Blistering of Langmuir-Blodgett Bilayers Containing Anionic Phospholipids as Observed by Atomic Force Microscopy. *Biophysical Journal* **77,** 1683–1693 (1999).

33. Prudovsky, I., Thallapuranam, S. K., Sterling, S. & Neivandt, D. Protein-Phospholipid Interactions in Nonclassical Protein Secretion: Problem and Methods of Study. *International journal of molecular sciences* **14,** 3734–3772 (Feb. 2013).

34. Matsuzaki, K. Why and how are peptide–lipid interactions utilized for self-defense? Magainins and tachyplesins as archetypes. *Biochimica et Biophysica Acta (BBA) - Biomembranes* **1462,** 1–10 (1999).

35. Park, C. B., Kim, H. S. & Kim, S. C. Mechanism of action of the antimicrobial peptide buforin II: Buforin II kills microorganisms by penetrating the cell membrane and inhibiting cellular functions. *Biochemical and Biophysical Research Communications* (1998).

36. Brogden, K. A. Antimicrobial peptides: pore formers or metabolic inhibitors in bacteria? *Nature Reviews Microbiology* **3,** 238 (Mar. 2005).

37. Yeaman, M. R. Mechanisms of Antimicrobial Peptide Action and Resistance. *Pharmacological Reviews* **55,** 27–55 (2003).

38. Vishnepolsky, B. & Pirtskhalava, M. Prediction of linear cationic antimicrobial peptides based on characteristics responsible for their interaction with the membranes. eng. *Journal of chemical information and modeling* **54,** 1512–1523 (May 2014).

39. Sakho, E. H. M., Allahyari, E., Oluwafemi, O., Thomas, S. & Kalarikkal, N. in *Thermal and Rheological Measurement Techniques for Nanomaterials Characterization* 37–49 (Dec. 2017).

40. Günther Crolly. *Hydrodynamic diameter* 2019. `https://www.fritsch-international.com/particle-sizing/fritsch-knowledge/hydrodynamic-diameter/`.

41. Gibb, T. & Ayub, M. in *Micro and Nano Technologies* (eds Edel, J. B. & Albrecht, T. B. T. .-.-. E. N. f. B. A.) 121–140 (William Andrew Publishing, Oxford, 2013). `http://www.sciencedirect.com/science/article/pii/B9781437734737000054`.

42. Burnett, T. L. *et al.* Large volume serial section tomography by Xe Plasma FIB dual beam microscopy. *Ultramicroscopy* **161,** 119–129 (2016).

43. Beis, K., Whitfield, C., Booth, I. & Naismith, J. H. Two-step purification of outer membrane proteins. *International Journal of Biological Macromolecules* **39,** 10–14 (Aug. 2006).

44. Lind, T. K. *et al.* Formation and Characterization of Supported Lipid Bilayers Composed of Hydrogenated and Deuterated Escherichia coli Lipids. *PLOS ONE* **10,** e0144671 (Dec. 2015).

45. Klinkenberg, J. Extraction of Chloroplast Proteins from Transiently Transformed Nicotiana benthamiana Leaves. *Bio-protocol* **4,** e1238 (2014).

46. Klinkenberg, J. *et al.* Two Fatty Acid Desaturases, STEAROYL-ACYL CARRIER PROTEIN Δ^9-DESATURASE6 and FATTY ACID DESATURASE3, Are Involved in Drought and Hypoxia Stress Signaling in Arabidopsis Crown Galls. *Plant Physiology* **164,** 570 LP –583 (Feb. 2014).

47. Avanti Polar Lipids. *TLC-solvent-systems* 2019. `https://avantilipids.com/tech-support/analytical-procedures/tlc-solvent-systems`.

48. Zuidam, J. N., Vrueh, d. R. & Crommelin, J. D. in *Liposomes* (eds Torchilin, P. V. & Weissig, V.) Torchilin, 31–77 (Oxford University, 2007).

49. Hope, J., Nayar, R. R., Mayer, L. D. & Cullis, P. R. *-REDUCTION OF LIPOSOME SIZE AND PREPARATION OF UNILAMELLAR VESICLES BY EXTRUSION TECHNIQUES* in (2002).

50. Ong, S. G. M., Chitneni, M., Lee, K. S., Ming, L. C. & Yuen, K. H. Evaluation of Extrusion Technique for Nanosizing Liposomes. eng. *Pharmaceutics* **8,** 36 (Dec. 2016).

51. Chibowski, E. & Szcześ, A. Zeta potential and surface charge of DPPC and DOPC liposomes in the presence of PLC enzyme. *Adsorption* **22,** 755–765 (2016).

52. Richter, R., Mukhopadhyay, A. & Brisson, A. Pathways of lipid vesicle deposition on solid surfaces: a combined QCM-D and AFM study. eng. *Biophysical journal* **85,** 3035–3047 (Nov. 2003).

53. Avantii Polar Lipids. *Phase Transition Temperatures for Glycerophospholipids* 2019. `https://avantilipids.com/tech-support/physical-properties/phase-transition-temps/`.

54. Márquez, I. F. & Vélez, M. Formation of supported lipid bilayers of charged E. coli lipids on modified gold by vesicle fusion. *MethodsX* **4,** 461–468 (Nov. 2017).

55. Cai, L., Zhu, L. & Liu, Q. Formation of MspA channel on Nanopore-Spanning Lipid Bilayer. *IOP Conference Series: Materials Science and Engineering* **394,** 022067 (Aug. 2018).

56. Ries, R., Choi, H., Blunck, R., Bezanilla, F. & Heath, J. Black Lipid Membranes: Visualizing the Structure, Dynamics, and Substrate Dependence of Membranes. *The Journal of Physical Chemistry B* **108** (Oct. 2004).

57. Richter, R. P. & Brisson, A. R. Following the formation of supported lipid bilayers on mica: a study combining AFM, QCM-D, and ellipsometry. eng. *Biophysical journal* **88,** 3422–3433 (May 2005).

58. Demarche, S., Sugihara, K., Zambelli, T., Tiefenauer, L. & Vörös, J. *Techniques for recording reconstituted ion channels* 1077–1089 (Mar. 2011).